Elsevier Editorial System(tm) for Chemical Engineering Science
Manuscript Draft

Manuscript Number: CES-D-14-00122R1

Title: Investigation of flow hydrodynamics and regime transition in a gas-solids fluidized bed with different riser diameters

Article Type: Regular Article

Keywords: Flow regime, Electrical capacitance tomography, Differential pressure, Solids volume fraction, Bubble characteristic, Transition velocity

Corresponding Author: Prof. HaiGang Wang, Ph.D.

Corresponding Author's Institution: Chinese Academy of Sciences

First Author: Guizhi Qiu, PhD

Order of Authors: Guizhi Qiu, PhD; Jiamin Ye, PhD; HaiGang Wang, Ph.D.; Wuqiang Yang, PhD

Abstract: It is important to understand the flow hydrodynamics behavior of a circulating fluidized bed (CFB) reactor for efficient operation. The objective of this research is to identify and characterize the flow regimes in a fluidized bed with different riser diameters. For this purpose, electrical capacitance tomography (ECT) combined with pressure measurement has been used to investigate the flow characteristics and flow regime transitions. Experiment was carried out in a cold gas-solids fluidized bed to investigate the flow regimes and the transition velocities. Three risers of different diameter, 10, 12 and 15 cm, are designed and used for comparison. A twin-plane ECT sensor and a differential pressure transducer are used to obtain the solids volume fraction and differential pressure in the bottom region. Different flow regimes including bubbling, slugging and turbulent flow regime were formed with two distinct transition velocities. The flow characteristics are investigated in terms of solids volume fraction, bubble diameter and bubble rising velocity. The transition velocities are compared based on the ratio of the static bed height to bed diameter (Hst/D) and the measured position (i.e. the axial position and radial position).

***Cover Letter**

16 January 2014

Dr. Haigang Wang
Institute of Engineering Thermophysics
Chinese Academy of Sciences
P O Box 2706
11 Beisihuaixi Road
Beijing, 100190
China
Tel: +0086 10 82543140
Fax: +0086 10 82543119
E-mail: wanghaig@hotmail.com

Dear Editor,

As Chemical Engineering Sciences is well known in publishing high quality scientific papers in the research field of chemical engineering and multiphase flows, we hope to publish our recent work on the investigation of gas-solid circulating fluidized bed with a diameter changing riser by electrical capacitance tomography and pressure measurements. The manuscript title is "Investigation of flow regimes in a gas-solids fluidized bed with a riser of changing diameter".

In the literature, there are many reports on flow hydrodynamics research in fluidized beds with conventional riser. However, the coal gasification process presents some challenges to a conventional CFB, such as low solids holdup, inhomogeneous solids distribution and short residence time. In this paper, a new fluidized bed with diameter changing riser is designed and used in the coal gasification process. The flow characteristics are investigated in terms of solids volume fraction and distribution, bubble diameter and bubble rising velocity based on capacitance tomography and pressure measurements. The transition velocities are compared based on the ratio of the height of static bed to bed diameter (H_{st}/D) and the measured position (i.e. the axial position and radial position). The results provide valuable information for the operation in a fluidized bed with diameter changing riser.

The content of the manuscript is original and unpublished and is not being considered for publication elsewhere.

Thank you very much for your consideration
I look forward to hearing from you.

Yours sincerely,

Haigang Wang

Reply to reviewers

We would like to thank the editor and reviewers for their helpful comments. According to the comments, we have made all changes and marked in red for the first Reviewer and blue for the second Reviewer in the manuscript, which are summarized as follows.

First Reviewer Comments:

Comment 1: The title of this paper is not proper.

Answer: The title of this paper has been changed to "Investigation of flow hydrodynamics and regime transition in a gas-solids fluidized bed with different riser diameters".

Comment 2: Introduction: The originality of this paper could be the measurement of the transition velocities for a riser. However, the references are not focused on the pints around the originality of this paper at all. This reviewer cannot obtain the substantial point because the references are very very broad.

Answer: We have added some sentences for the above comment (marked in red in the manuscript) and summarized as follows.

Line 15 to 18 in the third paragraph on page 2, "Johnsson *et al.* (2000) and Makkawi *et al.* (2002) studied …".
Line 1 to 5 in the last paragraph on page 2, "However, most of the previous researches …".
Line 8 to 10 in the last paragraph on page 2, "Ellis *et al.* (2004) found that …".

Comment 3: Introduction: The motivation in this study is very very week. "few reports on the transition velocities for a riser with changing diameter" is not motivation for high this high level international journal. It needs more scientific reasons to lead to the motivation. This reviewer cannot understand the scientific or engineering reason of three types of riser diameter. This author should describe the reason from the view point of two phase flow dynamics.

Answer: We have added some sentences for the above comment and summarized as follows.

Line 2 to 3 in the last paragraph on page 1 and line 1 to 2 in the first paragraph on page 2, "It provides good gas-solids mixing …".
Line 1 to 6 in the second paragraph on page 2, "However, due to the change in …".
Line 1 to 4 in the first paragraph on page 3, "Although considerable research efforts …".

Comment 4: Deviation of the particles diameter are missing. The reviewer think the sands are not proper for discussion of dynamics because the properties of each sand particle are not uniform.

Answer: The particles used in this study are sands (mixture of Group B particles) with a mean diameter of 469 μm and the particle size distribution is shown in Fig. 3. The details are shown in section 2.5 on page 5, "The particles used in this study …".

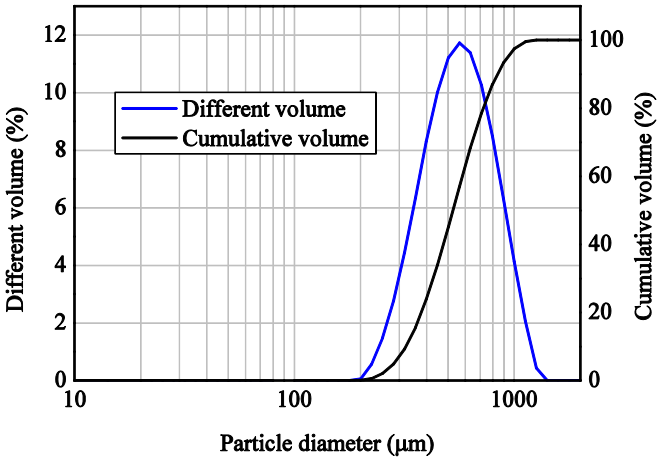

Fig. 3 Particle size distribution

Comment 5: The roots blower has air velocity fluctuation. How to reduce it or how the fluctuation affects the experimental results of two phase flow velocity?

Answer: In this study, the effect of the airflow fluctuation on the gas-solids flow hydrodynamics in the riser can be neglected. We have added the details in line 4 to11 in the second paragraph on page 3, "Airflow at ambient temperature is introduced to the riser to fluidize the particles through a trefoil Roots blower and a wire gauze air distributor. A plenum chamber is designed below the air distributor to provide a uniform air distribution over the whole cross-section of the riser and to maintain a turbulence-free airflow (Depypere *et al*. 2004). The Airflow is manually controlled by using two bypass valves located downstream of the blower assisted by operating frequency fine-tuning and the percentage deviation of airflow was less than 5 %. The pipe from the Roots blower to the plenum chamber, with a length of about 20 m, can weaken the influence of airflow fluctuation. Therefore, the effect of the airflow fluctuation on the gas-solids flow hydrodynamics in the riser can be neglected."

Comment 6: In order to measure the velocity between the two planes, the flow should be totally assumed a steady two phase flow without any acceleration. This reviewer does not agree with the steady two phase flow in this fields because of the air flow fluctuation and the gravity, Saffman and Magnus lift forces on the particles and so on.

Answer: The gap between the two ECT planes is 2 cm. In this study, it is assumed that the bubbles do not undergo too much transformation from one measuring plane to the next. And the ECT data

acquisition rate (60 frames per second) is high enough to give accurate measurement results for the bubble rising velocity.

The details are shown in line 2 to 10 in the first paragraph of section 3.2.4 on page 11, "The relationship between …".

For the comment: This reviewer does not agree with the steady two phase flow in this fields because of the air flow fluctuation and the gravity, Saffman and Magnus lift forces on the particles and so on.

We are agreed with the reviewer comment and added one paragraph to give the explanation in the first paragraph on page 12, "The hydrodynamic behaviour in a gas-solids fluidized bed is a complex flow system and it is unstable due to particle acceleration, gravity and many other forces. The correlation calculation based on the ECT signals only give a rough estimate of the bubbling rising velocity and further work is necessary to address the above factors which affect the predicted accuracy for bubbling rising velocity."

Comment 7: The reconstruction images are strongly dependent on the relaxation values of Landweber method. This manuscript has to describe the point.

Answer: We have added some sentences to give details for relaxation values in section 2.3.

The details for the relaxation factor (τ) are shown in the fifth paragraph on page 4, "In Eq. 1, τ is …". The details for the step length or gain factor (α) are shown in the sixth paragraph on page 4, "In Eq. 1, α is …".

Comment 8: The image acquisition rate for the twin-plane ECT sensor is 60 frames/second. This manuscript should describe this method measure volume fraction under this frame rate. Strictly speaking, it is not volume fraction during the frame rate.

Answer: The image acquisition rate for each plan of the twin-plane ECT sensor is 60 frames per second (line 9 to 10 in the first paragraph on page 4). More details can be found in section of 3.2 on page 4 and 5.

Comment 9: The reviewer guesses ECT measurement includes noise. This manuscript should describe the measurement capacitance is accurate, the physical reason, and how the electrodes are earthen. The detail information is totally missing in this section.

Answer: The AC-ECT system used in this research has high signal-to-noise ratio (SNR) which used to indicate the signals quality (Yang and York 1999). Moreover, low-pass-filter is used to eliminate the

noise effect on the signals to improve the image quality (Wang et al. 2009) The DC power supply provides the earth or ground for shielding the electrodes to eliminate the noise effect from environment.

The details are given in line 5 to 9 in the first paragraph on page 4.

Comment 10: Many experimental conditions are missing. The flow pattern in fluidized bed depends on solid gas ratio, particle Geldart type and so on. Also, how ECT does the calibration?

Answer: The detailed experiment conditions are summarized in Table 1 (section 2.5 on page 5).

Table 1 Summary of the experimental operation conditions

Experimental unit	Operating conditions
Riser	D = 10 cm, 12 cm, 15 cm, height = 3.0 m
Distributor	Material: wire gauze, 100 mesh, Z = 0
Fluidizing gas	Air at ambient conditions
Superficial gas velocity	0.4-4.5 m/s for 10 cm D., 0.25-3.5 m/s for 12 cm D., 0.2-3.0m/s for 15 cm D.
Particle	Material: sand, mean diameter = 469 μm, bulk density = 1608 kg/m^3
Static bed height	20 cm, 25 cm
ECT system	Plane 1: Z = 2.5-8.5 cm, plane 2: Z = 10.5-16.5 cm, eight electrodes per plane
DP transducer	Z = 2.5-16.5 cm

* Z means the axial height above the distributor

The particles used in this study are mixture of Group B particles and the close-packing volume fraction is 0.54. The details are shown in section 2.5 on page 5, "The particles used …".

To normalize the measurement capacitance of C_M by Eq. 4, high and low calibrations need to be performed to get the capacitance data of C_H and C_L before the experiment. In this research, the high calibration is done by filling the ECT sensor with sands used in the experiment and the measured capacitance is saved as C_H. And the low calibration is done by empting the ECT sensor with air and the measured capacitance is saved as C_L. We have added these sentences in thethird paragraph on page 5, "To normalize the measurement capacitance of C_M by Eq. 4…".

Comment 11: G is the normalized grey level vector. This terminology is very unclear for normal reader in this field. Use the physical terminology.

Answer: G is the normalized permittivity distribution, which is often called grey level vector in image reconstruction to indicate the percentage occupied by particles. We have added this sentence in the third paragraph on page 4.

Comment 12: I hope you could polish the manuscript more after 3.1.1 section

Answer: We have rewritten and refined the English writing carefully through the whole manuscript.

Second Reviewer Comments:

Comment 1: In Nomenclature inner riser diameter is depicted as D, on Fig. 1 as ID. It could be the unified.

Answer: The inner riser diameter has been unified as D.

Comment 2: Fluidized bed height could be shown on Fig. 1.

Answer: The height of riser bottom and two static bed heights are all shown in Fig. 1.

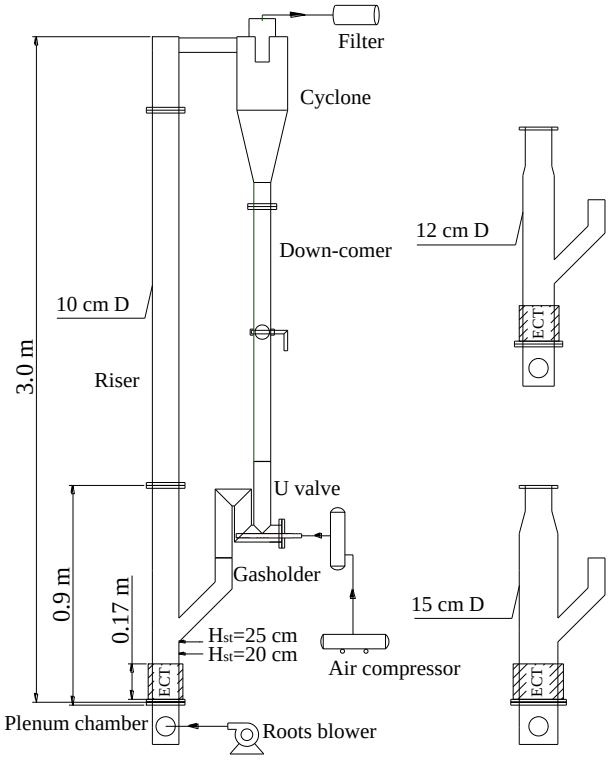

Fig. 1 Circulating fluidized bed

Comment 3: ECT sensor was fabricated using self-adhesive copper tape put outside acrylic riser. Wall thickness of the riser could be mentioned. However more systematic experiments aimed directly at elucidating this wall effect would be need.

Answer: We have added some sentences to give details for the above comment in line 3 to 6 in the last paragraph on page 3 "The riser wall is made of cast acrylic with thickness of 0.5 cm. Chaplin et al. (2005) indicated that the possible influence of the permittivity of the acrylic cone wall is negligible. In

addition, the wall effect on the capacitance has been compensated in the low and high calibrations which are used to normalize the measured capacitances (Yang and York 1999).”

Comment 4: Figures 4 and 6 show different charts of power spectra. The scales of graphs were set in such a way, that graphs look very similar, although vertical axis values are different, but close each to other. Therefore it is difficult to visually compare charts, especially adjacent horizontal ones. Let authors consider make vertical axes values equal. Graphs will still be clear but will better reflect comments in text (3.1.1 and 3.1.2). Similarly on Fig. 6, 20x10E12 equals to 2x10E13. It could be unified.

Answer: In Figs. 5 and 7 (original Figs. 4 and 6), the adjacent horizontal graphs have been set with the same axis value.

Comment 5: Text in 3.2.1 - second paragraph should be changed from: "The profiles of (beta) ..... with the superficial gas velocity is shown" to: "The profiles of (beta) ..... with the superficial gas velocity are shown"

Answer: We have changed.

Comment 6: The title of the paper suggests special construction of the riser, f. ex. conical shape with "changing diameter". Let the authors consider change of the title f. ex to: "Investigation of flow regimes in a gas-solids fluidized bed with (eventually for) risers of different diameters"

Answer: The title of this paper has been changed to be “Investigation of flow hydrodynamics and regime transition in a gas-solids fluidized bed with different riser diameters”.

Other changes in the manuscript:

(1) We have rmoved the image reconstruction part into section 2.3 to give details information for the ECT image reconstruction.
(2) We have added new references (marked in red in the reference list) to support the content changes in the manuscript.

Graphical Abstract (for review)

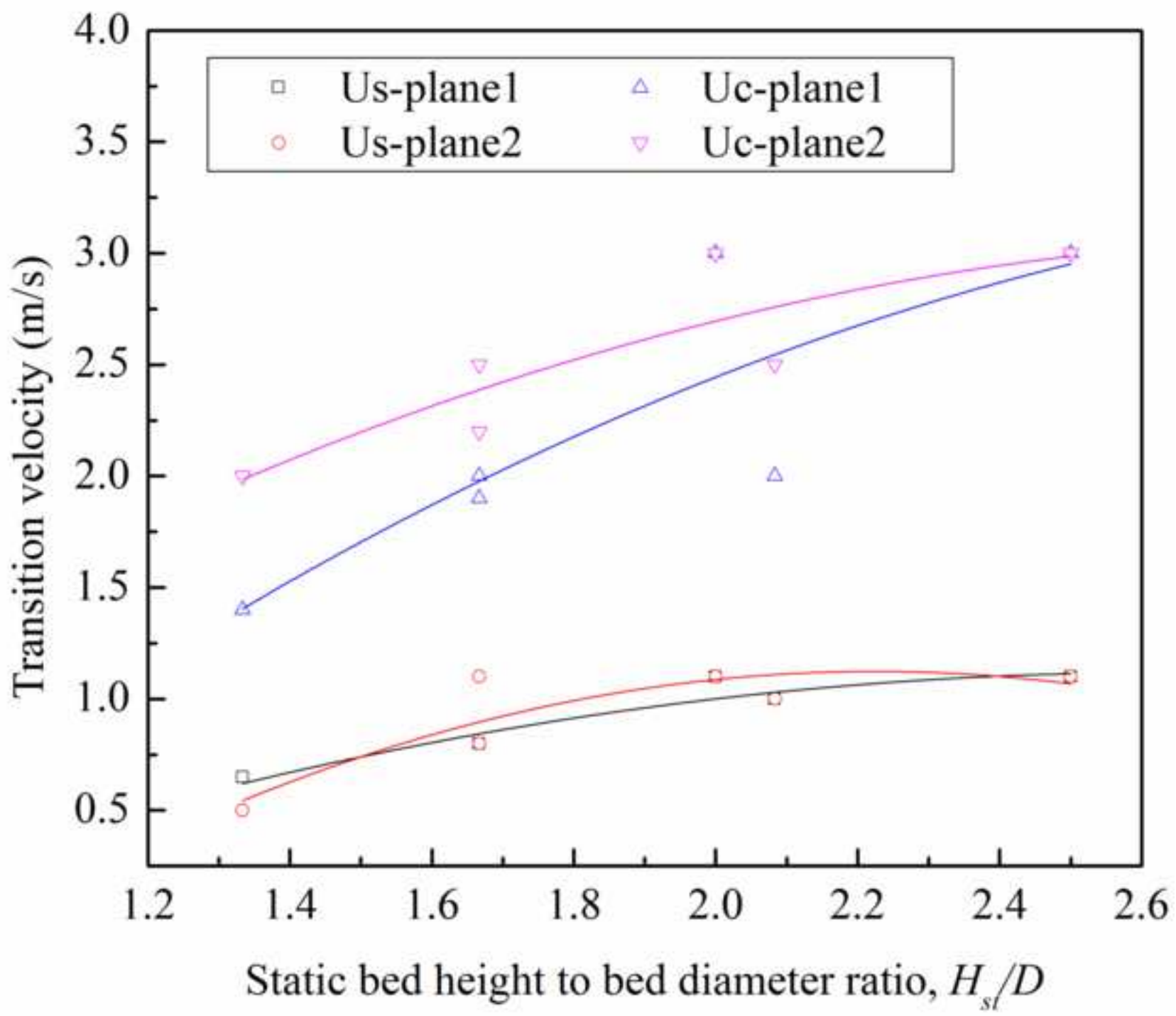

Highlights

- Fluidized bed with diameter changing riser is designed for coal gasification
- ECT is used to investigate the gas-solid flow in the CFB system
- H_{st}/D affects the transition velocities in the diameter changing riser

Submitted to *Chemical Engineering Science* (Revised Version 25 Apr. 2014)

Investigation of flow hydrodynamics and regime transition in a gas-solids fluidized bed with different riser diameters

Guizhi Qiu[1,2], Jiamin Ye [1], Haigang Wang [1*], Wuqiang Yang[3]

[1.] Institute of Engineering Thermophysics, Chinese Academy of Sciences, PO Box 2706, Beijing 100190, China

[2.] University of Chinese Academy of Sciences, PO Box 2706, Beijing 100190, China

[3.] School of Electrical and Electronic Engineering, The University of Manchester, Sackville Street, Manchester M13 9PL, UK

Abstract: It is important to understand the flow hydrodynamics behavior of a circulating fluidized bed (CFB) reactor for efficient operation. The objective of this research is to identify and characterize the flow regimes in a fluidized bed with different riser diameters. For this purpose, electrical capacitance tomography (ECT) combined with pressure measurement has been used to investigate the flow characteristics and flow regime transitions. Experiment was carried out in a cold gas-solids fluidized bed to investigate the flow regimes and the transition velocities. Three risers of different diameter, 10, 12 and 15 cm, are designed and used for comparison. A twin-plane ECT sensor and a differential pressure transducer are used to obtain the solids volume fraction and differential pressure in the bottom region. Different flow regimes including bubbling, slugging and turbulent flow regime were formed with two distinct transition velocities. The flow characteristics are investigated in terms of solids volume fraction, bubble diameter and bubble rising velocity. The transition velocities are compared based on the ratio of the static bed height to bed diameter (H_{st}/D) and the measured position (i.e. the axial position and radial position).

Keywords: Flow regime, Electrical capacitance tomography, Differential pressure, Solids volume fraction, Bubble characteristic, Transition velocity

1. Introduction

Circulating fluidized bed (CFB) reactors have been widely used in industrial processes, including coal combustion, biomass pyrolysis, coal gasification, and catalytic cracking. It provides good gas-solids mixing and excellent heat and mass transfer properties. The reactor performance is significantly depended on the

[*] Correspondence author, Tel.: 0086-10-82543140, E-mail: wanghaig@hotmail.com (H.G. Wang)

dynamics properties of the gas-solids two-phase flow system (Davidson *et al*. 1985). According to the characteristics of gas-solid fluctuations, the fluidization behavior has been widely classified into several flow regimes, including the bubbling, slugging, turbulent and fast fluidization flow regime (Johnsson *et al*. 2000, Svensson *et al*. 1996, Zijerveld *et al*. 1998).

However, due to the change in dimensions and geometrical parameters, i.e. CFB riser's chamber shape and diameter, the flow hydrodynamics and regime transition will be different from each other which results in the change of heat and mass transfer characteristics (Kim *et al*. 2004). Furthermore, the flow regime transition is strongly depended on the diameter of riser and operating condition (Shaul *et al*. 2012). For process optimization and scale-up purposes, it is necessary to investigate the flow behavior and different flow regime transitions in a fluidized bed with different riser diameters.

In general, the flow regimes can be identified by standard deviation and frequency spectrum of measured parameters, such as pressure drop (Bai *et al*. 1996a, Johnsson *et al*. 2000, Monazam *et al*. 2005, Piskova and Mörl 2008). Fan *et al*. (1983) characterized the flow regimes by measuring the bubble rising velocity using pressure fluctuation signals. The solids volume fraction has also been widely used to analyze the flow regime and it can be measured by intrusive techniques such as a momentum probe (Azzi *et al*. 1991, Bai *et al*. 1996b), a capacitance probe (Hage *et al*. 1996, Wiesendorf and Werther 2000) and an optical fiber probe (Cui *et al*. 2001, Ellis *et al*. 2004). However, it is difficult to measure the flow variations in a cross section simultaneously which is a key to optimize the process operation in a fluidized bed, especially in a large-scale fluidized bed (Wang *et al*. 2006). As a reliable non-invasive technique, electrical capacitance tomography (ECT) can present the cross-sectional images for measuring the solids volume fraction and analyzing the flow behavior (Dyakowski *et al*. 1997, Lehner and Wirth 1999, Malcus *et al*. 2000). Numerous research studies have been reported on the analysis of flow regime characteristics in fluidized beds based on ECT measurements (Du *et al*. 2005, Malcus *et al*. 2000, Makkawi and Wright 2002, Srivastava *et al*. 1998, Wang *et al*. 1995). Du *et al*. (2005) studied the bubble characteristics by the quasi-three dimensional flow structures of a gas-solid fluidized bed using ECT. Johnsson *et al*. (2000) and Makkawi *et al*. (2002) studied the identification of flow regimes and the results indicated that the dominant frequency reached a minimum at the transition point from bubbling to slugging flow regime, while the standard deviation reached a maximum at the transition point from slugging to turbulent flow regime.

However, most of the previous researches are focused on the flow hydrodynamics characteristics and little attention has been paid to the factor which influences the transition velocity. Bai *et al*. (1996a) pointed out that the transition velocity was influenced by many factors including measured position and bed geometries. Rhodes *et al*. (1998) confirmed that different flow regimes existed along the riser based on the analysis of the gas-solids flow behavior both in the bottom and the top region. Du *et al*. (2005) studied the effect of the bed diameter on the transition velocity from slugging to turbulent flow regime. It indicated that the transition velocity decreases with the increase of bed diameter. Ellis *et al*. (2004) and Shaul *et al*. (2012) generalized the transition velocity based on the height to bed diameter ratio. Ellis (2004) found that the transition velocity from slugging to turbulent fluidization flow regime increased with the ratio of bed height to bed diameter.

Although considerable research efforts have been made in the analysis of fluidized bed hydrodynamic, a systematic study on the gas-solids flow dynamic characteristics, especially the flow regime transition, is still necessary to optimize the design and process operation for a circulating fluidized bed with different riser diameters. In this research, the gas-solids hydrodynamics flow structure in the bottom of CFB risers with different diameter has been studied based on ECT measurements combined with differential pressure fluctuations analysis. The ultimate objectives of this research are: (1) to understand the flow behavior in a gas-solids fluidized bed with different riser diameters based on key process parameters, (2) to investigate the flow regime characteristics, including the solids volume fraction, bubble diameter and bubble rising velocity, and (3) to study the effect of riser diameter, static bed height and measured position on the transition velocity.

2. Experiment

2.1 Experimental setup

Fig. 1 shows the experimental setup of a gas-solids circulating fluidized bed, which consists of a riser of 3.0 m in height, a cyclone and a non-mechanical U-valve. The entire system is made of cast acrylic except for a steel cyclone separator. The bottom of the riser is designed with three different inside diameters (10, 12 and 15 cm). Airflow at ambient temperature is introduced to the riser to fluidize the particles through a trefoil Roots blower and a wire gauze air distributor. A plenum chamber is designed below the air distributor to provide a uniform air distribution over the whole cross-section of the riser and to maintain a turbulence-free airflow (Depypere *et al*. 2004). The Airflow is manually controlled by using two bypass valves located downstream of the blower assisted by operating frequency fine-tuning and the percentage deviation of airflow was less than 5 %. The pipe from the Roots blower to the plenum chamber, with a length of about 20 m, can weaken the influence of airflow fluctuation. Therefore, the effect of the airflow fluctuation on the gas-solids flow hydrodynamics in the riser can be neglected. The superficial gas velocity is measured by a turbine flow meter and adjusted to correct the change in temperature and pressure in the plenum chamber. Particles are carried upwards in the riser and exit from the top through a right-angled tube connected to a cyclone where particles are separated from the gas phase. Particles separated by the cyclone are fed back to the bottom of the riser through the U-valve as shown in Fig. 1.

<Figure 1>

2.2. ECT sensor design

Fig. 2 shows the structure of the ECT sensor used in this research. It consists of two planes (plane 1 and plane 2). Each plane has eight electrodes made of self-adhesive copper tape. The electrodes are stuck to the outside wall of the riser and covered by shielding copper to eliminate external interference. The riser wall is made of cast acrylic with thickness of 0.5 cm. Chaplin *et al*. (2005) indicated that the possible influence of the permittivity of the acrylic cone wall is negligible. In addition, the wall effect on the capacitance has been compensated in the low and high calibrations which are used to normalize the measured capacitances (Yang

and York 1999). The mid-positions of plane 1 and plane 2 locate at 13.5 cm and 5.5 cm above the air distributor respectively. The length of the electrodes is 6 cm. The widths of the electrodes are 3.5, 4.0 and 5.0 cm for the three risers with different diameter 10, 12 and 15 cm, respectively. An AC-based electrical capacitance tomography (AC-ECT) system with 16 channels (Yang and York 1999) is employed for the experiments. The DC power supply provides the earth or ground for shielding the electrodes to eliminate the noise effect from environment. The AC-ECT system used in this research has a high signal-to-noise ratio (SNR) which used to indicate the signals quality (Yang and York 1999). Moreover, low-pass-filter is used to eliminate the noise effect on the signals to improve the image quality (Wang *et al*. 2009). The image acquisition rate for each plan of the twin-plane ECT sensor is 60 frames per second and the number of data acquisition is set to be 10,000 for each measurement.

<Figure 2>

2.3. Image reconstruction

An optimized iterative algorithm based on the Landweber method is used for image reconstruction (Liu *et al*. 1999). The reconstructed image is divided into 64×64 grids, which results in 3001 effective pixels in the circular cross section or measurement area in the riser. The optimized iterative algorithm is expressed as

$$G^{j+1} = G^{j} \cdot (1.0 + \tau) + \alpha \cdot S^{T} \cdot (\lambda - S \cdot G^{j}) \cdot (1 - \tau) \tag{1}$$

where G is the normalized permittivity distribution, which is often called grey level vector in image reconstruction to indicate the percentage occupied by particles. G^j is G obtained in *j-th* iteration. G^0, the first matrix of G^j, is calculated by Linear back projection (LBP) and expressed as

$$G^{0} = \frac{S^{T}\lambda}{S^{T}u_{\lambda}} \tag{2}$$

where S is the sensitivity matrix for the ECT sensor, u_λ is an identity vector, λ is the normalized capacitance vector calculated by Eq. 4. The detail for the calculation of sensitivity matrix of S is given in reference (Kim *et al*. 2007).

In Eq. 1, τ is a relaxation factor. There are no general rules for choosing the best value for the relaxation factor. The optimum value depends on a number of factors, e.g. the nature of the problem, the number of grid points, the grid spacing, and the iteration procedure used (Wang and Yang 2010). In this paper, the value of τ is 0.005.

In Eq. 1, α is a step length or gain factor, which a suitable size of the gain factor can be estimated to be (Yang *et al*. 1999)

$$\alpha = 2 / m_{\max} \tag{3}$$

where m_{max} is the maximum eigenvalue of $S^T S$.

In Eq. 2, λ is calculated by

$$\lambda = \frac{C_M - C_L}{C_H - C_L} \tag{4}$$

where C_M is the measurement capacitance vector, C_H and C_L represent the capacitance vector measured in close-packing and empty bed respectively. To normalize the measurement capacitance of C_M by Eq. 4, high and low calibrations need to be performed to get the capacitance data of C_H and C_L before the experiment. In this research, the high calibration is done by filling the ECT sensor with sands used in the experiment and the measured capacitance is saved as C_H. And the low calibration is done by empting the ECT sensor with air and the measured capacitance is saved as C_L. A detailed calibration procedure is given in reference (Yang and York 1999).

2.4. Pressure acquisition

A differential pressure transducer (Setra 268110KLD11FF2NN) is used to measure the pressure drop of the corresponding zone of the twin-plane ECT sensor. Two pressure taps are installed along the riser wall located at 2.5 cm and 16.5 cm above the air distributor and connected to the differential pressure transducer, which is interfaced with a PC for data acquisition. In this work, the data acquisition rate is set as 170 samples per second and the data acquisition time is100 seconds.

2.5. Experiment conditions and materials

The particles used in this study are sands (mixture of Group B particles, according to Geldart classification (Geldart 1973)) with a mean diameter of 469 μm and the particle size distribution is shown in Fig. 3. The bulk density is 1608 kg/m^3 and the close-packing volume fraction is 0.54. Experiments are carried out with two static bed heights (H_{st} = 20 cm and 25 cm), which are marked in Fig. 1. The detailed experiment conditions are summarized in Table 1.

<Figure 3>

<Table 1>

3. Results and discussion

3.1 Flow regime identification

3.1.1 Time and frequency domain analysis on solids volume fraction

Time and frequency domain analysis are the most common approach to describing the dynamic behavior in a gas-solids flow system and defining the flow regime transition (Makkawi and Wright 2002, Piskova and Mörl 2008). In this research, the solids volume fraction is analyzed in terms of standard deviation, auto-correlation function and power spectrum.

The area-averaged solids volume fraction in a cross section, β, is calculated by

$$\beta = \vartheta \cdot \overline{G} = \vartheta \cdot \frac{\sum_{i=1}^{M} G_i \cdot a_i}{\sum_{i=1}^{M} a_i} \tag{5}$$

where θ is the close-packing volume fraction of experimental material, which is 0.54 in this research, G is the normalized permittivity distribution calculated by Eq. 1, a is the effective pixel area and M is the effective pixel number inside the circular imaging area, which is 3001.

The standard deviation (SD) of β is defined as

$$\mathrm{SD} = \sqrt{\frac{1}{N-1}\sum_{i=1}^{N}(\beta_i - \overline{\beta})^2} \tag{6}$$

where, β_i is a time series of β, and $\overline{\beta}$ is the time-averaged of β_i, N is the total number of measurements, which is 10,000.

To quantify the temporal patterns, the auto-correlation function between two points separated by a time lag, k times Δt, is calculated by (Johnsson *et al*., 2000)

$$c_{xx}(k) = \sum_{n=0}^{N-|k|-1}(\beta_i - \overline{\beta})(\beta_{i-k} - \overline{\beta}) \tag{7}$$

The auto-correlation function is normalized with the value at zero lag, $c_{xx}(0)$, thus

$$C_{xx}(k) = \frac{c_{xx}(k)}{c_{xx}(0)} \tag{8}$$

i.e. $-1 \leq C_{xx} \leq 1$.

The results obtained from the ECT plane 1 for the riser of 10 cm in diameter (H_{st} = 25 cm) are shown in Fig. 4, including the time domain analysis on area-averaged solids volume fraction, β. Three different flow regimes can be identified from Fig. 4: (1) bubbling flow regime, (2) slugging flow regime and (3) turbulent fluidization flow regime. Fig. 4 (a) shows the average solids volume fraction fluctuations under different superficial gas velocities. It can be found that β varies (significantly different in amplitude and frequency) with time periodically for each superficial gas velocity. Fig. 4 (b) shows the standard deviation and the dominant frequency, which is obtained by power spectra analysis as shown in Fig. 5, against the superficial gas velocity. With a low superficial gas velocity, the standard deviation increases with the superficial gas velocity and reaches a maximum at 2.5 m/s. This peak corresponds to the well-known transition velocity called $U_{C,}$ which is defined as the mark for the onset of turbulent fluidization regime (Bai *et al*. 1996b). The fluctuation of gas-solids flow reaches a maximum at U_C. With the further increase in superficial gas velocity, the standard deviation decreases dramatically due to the breakup of large bubbles.

Referencing the dominant frequency distribution as shown in Fig. 4 (b), it can be found that the fluctuation starts with a high frequency (2.0 Hz) and then decreases to a minimum (0.5 Hz) at U = 1.1 m/s, which marks the end of bubbling flow regime. This velocity is defined as the transition velocity from the bubbling to slugging flow regime, U_S. Another small peak on the standard deviation distribution can be observed at U_S due to the formation of a single large bubble.

Fig. 4 (c) illustrates the auto-correlation functions for three flow regimes. In the bubbling and turbulent fluidization flow regime, there is a periodic auto-correlation function on a scale and the frequency approximately equals to the corresponding dominant frequency. In the slugging flow regime, it can be seen that the decay in auto-correlation with time lag is fast. It indicates that the periodicity of the average solids volume fraction fluctuation is not significant in the slugging flow regime, which relates to the bubble dynamics.

Fig. 5 presents the power spectrum distribution calculated by Fast Flourier Transformation (FFT) for three flow regimes. It is clear that the bandwidth and amplitude vary considerably with the superficial gas velocity. Within the bubbling flow regime in Fig. 5 (a), a broad-band spectrum with low amplitude is observed, which indicates a distinguishable bubbling behavior. The dominant frequency is approximately 1 Hz. Fig. 5 (b) shows that the power spectrum for the slugging flow regime has a relatively narrow-banded spectrum with a high magnitude. This regime is governed by the dynamics of large bubbles and has much simpler signal fluctuation. The dominant frequency is relatively low (0.7 Hz). The power spectrum for the turbulent fluidization flow regime is shown in Fig. 5 (c). Compared with the slugging flow regime, the dominant frequency of turbulent fluidization flow regime is relatively high while the power spectrum magnitude is considerably low.

<Figure 4>

<Figure 5>

3.1.2 Analyses of differential pressure fluctuation

Fig. 6 shows the time domain analysis on the differential pressure fluctuations. Fig. 7 shows the power spectrum distribution for three flow regimes. Comparing Figs. 6 and 7 with Figs. 4 and 5, it can be found that the differential pressure fluctuation presents a similar behavior to the area-average solids volume fraction fluctuation. However, the transition velocities in Fig. 6 (b) (U_S' = 0.95 m/s and U_C' = 2.0 m/s) are slightly lower than those in Fig. 4 (b) (U_S = 1.1 m/s and U_C = 2.5 m/s), and the dominant frequencies are slightly higher than those of the average solids volume fraction fluctuation. One of the main reasons is that the ECT measurement represents the information on the whole cross section while the pressure probe only measures the near-wall region.

<Figure 6>

<Figure 7>

3.2 Gas-solids flow characteristics

To obtain the characteristics of the gas-solids flow, the solids volume fraction distribution and bubble characteristics obtained from the ECT sensor are further investigated.

3.2.1 Solids volume fraction distribution

The result obtained from ECT plane 1 is investigated in the riser of 10 cm in diameter with a static bed height of 25 cm. The solids volume fraction distribution is shown in Fig. 8.

The profiles of $\overline{\beta}$, $\overline{\beta}_{center}$ and $\overline{\beta}_{wall}$ with the superficial gas velocity are shown in Fig. 8 (a). The radial profile of the solids volume fraction averaged in time is shown in Fig. 8 (b). In Fig. 8 (a), $\overline{\beta}_{center}$ is the area-averaged value of $\overline{\beta}$ at the center (r/R < 0.07) and $\overline{\beta}_{wall}$ is the area-averaged value of $\overline{\beta}$ near the wall (r/R > 0.93). They are summarized from Fig. 8 (b) to investigate the maximum difference of solids volume fraction in the cross section. From Fig. 8 (a), it can be seen that $\overline{\beta}$, $\overline{\beta}_{center}$ and $\overline{\beta}_{wall}$ decrease with the superficial gas velocity. The gradients of trend lines of $\overline{\beta}$ for the three flow regimes show slightly increase. With the increase of superficial gas velocity, the difference between $\overline{\beta}_{wall}$ and $\overline{\beta}_{center}$ as a percentage of $\overline{\beta}$ increases from 9.7 % to

157 %. The above results indicate that the inhomogeneity of solids distribution in the cross section increases with the superficial gas velocity.

As shown in Fig. 8 (b), the solids volume fraction in the center is lower and increases monotonically along the radial direction towards the near wall region. In the bubbling flow regime (U < 1.1 m/s), the change in the solids volume fraction is relatively slow. The main reason is that the drag force is not strong enough to carry the highly concentrated solids in the bed when the bubble moves through the center. In the slugging flow regime (1.1 m/s < U < 2.5 m/s), the solids volume fraction in the center decreases significantly while that near the wall changes slowly. The solids volume fraction decreases by almost 40 % in the center and almost 13 % near the wall. In the turbulent fluidization flow regime, the radial profile of the solids volume fraction is similar to that of the slugging regime. The profile shows a smooth variation in the center (between r/R = 0 and r/R = 0.4) and a steep variation near the wall (between r/R = 0.4 and r/R = 1.0). This is a typical phenomenon, which can be seen in the turbulent fluidization flow regime since the gas-solids mixing increases due to the breakup of large bubbles.

<Figure 8>

3.2.2 Quasi-three-dimensional solids volume fraction distribution

Fig. 9 shows the quasi-three-dimensional distribution of solids volume fraction and the corresponding cross-sectional distribution for several typical superficial gas velocities. Each quasi-three-dimensional distribution is obtained by stacking 300 tomographic images within a consecutive period of 5 seconds. The vertical direction refers to the time. The horizontal direction refers to the diameter orientation from the top left to the bottom right of the cross-sectional images. The cross-sectional distribution in Fig. 9 represents the time-averaged solids volume fraction distributions. The color bar variation from blue to red stands for the increase of the solids volume fraction from low (empty bed) to high (close-packing).

The gas-solids flow analysis based on the quasi-three-dimensional solids volume fraction distribution is given as follows. The bubbles number in each figure stands for the frequency of bubbles through the ECT measured region, which related to bubble rising velocity. Fig. 9 (a) and (b) show the gas-solids flow behavior in the bubbling regime. A longer duration of pause between bubbles can be seen in Fig. 9 (a) and (b). In the slugging flow regime, as shown in Fig. 9 (c) and (d), there are significant differences in axial and radial distribution, compared with those in the bubbling flow regime. In addition, a growing number of bubbles can be seen and the average bubble diameter becomes larger. It should be noted that most particles tend to move to one side of the riser as a result of gas mal-distribution in plenum chamber caused by the single gas entrance at one side (Bhasker 2002). Fig. 9 (e) and (f) show the solids volume fraction distribution in the turbulent fluidization flow regime. This is the regime, in which small bubbles dominate the flow hydrodynamics. Within the cross section, the solids volume fraction in the center is much lower than that near the wall. In the meanwhile, very short duration of pause between bubbles can be observed from Fig. 9 (e) and (f).

<Figure 9>

3.2.3 Bubble diameter

Bubble size is one of the most important indexes in a fluidized bed reactor. Numerous of researches have been done in the 1970's and 1980's to investigate the bubble behavior in gas-solids fluidized beds. Darton (1977) generalized a semi-empirical model for bubble growth. The bubble diameter is defined as

$$D_b = 0.54(U - U_{mf})^{0.4}(h + 4\sqrt{\frac{A}{N_h}})^{0.8} / g^{0.2} \tag{9}$$

where D_b is the bubble diameter, h is the height of the bubble above the distributor, A is the cross-sectional area of the bed, N_h is the hole number of distributor, 0.54 is the experimentally determined constant. It was stated that this model is not applicable to slugging bed (Darton 1977).

The model defines a bubble as an area where the solids volume fraction is below a certain value. Wachem *et al*. (1998) choose this value to be 20 % of the close-packing volume fraction. When several bubbles exist in a cross section, D_b is the equivalent diameter of all bubbles in the measurement area.

Fig. 10 shows the bubble diameter obtained both by Eq. 9 and ECT for three different risers. It indicates that the bubble diameters measured by ECT plane 1 (the upper plane) are slightly larger than those obtained by Eq. 9, but they present a similar tendency with the superficial gas velocity. However, in ECT plane 2 (the lower plane), the bubble diameter measured by ECT is significantly larger than those by Darton's model. A possible reason is that the sensitivity of ECT sensor is lower in the center, which makes the ECT sensor difficult to detect small bubbles in the center.

It can be found that the measured bubble diameter in the slugging regime is different from that obtained by Eq. 9 (referencing in Fig. 10 (a): U = 1.1 m/s~2.5 m/s, Fig. 10 (b): U = 1.0 m/s~2.0 m/s and Fig. 10 (c): U = 0.8 m/s~1.9 m/s). It verifies that Darton's model is not applicable to the slugging regime.

In this research, the distributor is made of a wire mesh, which results in that the holes number in the distributor, N_h, is proportional to the cross-sectional area of the bed, A, in Eq. 9. Therefore, the bubble diameters of the three risers for the same superficial gas velocity obtained by Eq. 9 are essentially equal. This conclusion is confirmed by the ECT results that the bubble diameter has a similar value in the three different risers with the same superficial gas velocity, as shown in Fig. 10.

<Figure 10>

3.2.4 Bubble rising velocity

To investigate the bubble rising velocity, the measured results of the three different risers are analyzed using the cross-correlation method (Fan *et al*. 1983). The relationship between the signals of ECT plane 1 and plane 2 are quantified by the cross-correlation coefficient, which is used to estimate the time-lag for the bubble passing through the two planes. The gap between those two planes is 2 cm and the data acquisition rate for each plane is 60 frames per second. Compared with the bubble fluctuation frequency, i.e. less than 2.5 Hz (Fig. 4(b)), the ECT data acquisition rate is high enough to give accurate measurement results for the bubble rising velocity. It should be pointed out that the cross-correlation is only for the averaged bubbles crossing the measuring planes and it is assumed that the bubbles do not undergo too much transformation from one measuring plane to the next. The details for the calculation of the bubble rising velocity from the twin-plane ECT sensor are given by Liu *et al*. (2005).

The theoretical model proposed by Davidson and Harrison (1963) is

$$U_b = U - U_{mf} + 0.71\sqrt{gD_b} \tag{10}$$

where 0.71 is the analytically determined square root of the Froude number of a single rising bubble in an infinitely large homogeneous area in three dimensions.

The results of correlation analysis and bubble rising velocities obtained by ECT are shown in Fig. 11 (a), (c) and (e) for the three risers separately. The points with small correlation coefficients characterize that the correlation of gas-solids flow between the two adjacent planes is poor. There are two possible reasons: (1) different flow regimes exist in the two planes and (2) the gas-solids flow of the riser is unstable.

The bubble rising velocities obtained by Eq. 10 and ECT in the three risers are shown in Fig. 11 (b), (d) and (f) respectively. The bubble rising velocity obtained by Eq. 10 increases with the superficial gas velocity. The experimental results show the same distribution only in the bubbling regime for the three risers. In the bubbling regime, the bubble rising velocities obtained by Eq. 10 and ECT are approximately equal. In the slugging flow regime and turbulent fluidization flow regime, the bubble velocities become independent of the superficial gas velocity. This is consistent with the previous study by pressure fluctuation measurement (Fan *et al*. 1983). The difference between ECT measurements and the theoretical model can be explained that the visible flow rate is clearly lower than the excess gas velocity (U-U_{mf}) under normal operation conditions for bubble formation without slugging (Hilligardt and Werther 1986). Furthermore, in the turbulent fluidization flow regime there are several small bubbles in the cross section, while D_b is obtained based on the total area of bubbles instead of one bubble, thus the bubble rising velocity estimated by Eq. 10 is larger than the ECT measurement.

<Figure 11>

The hydrodynamic behavior in a gas-solids fluidized bed is a complex flow system and it is unstable due to particle acceleration, gravity and many other forces (Kariminpour and Pugsley 2011). In addition, the authors did not consider the bubble breakup and coalescence effect on the bubbling rising velocity when bubbles pass through the measuring planes (Wang and Yang 2011). The correlation calculation based on the ECT signals only give a rough estimate of the bubbling rising velocity and further work is necessary to address the above factors which affect the predicted accuracy for bubbling rising velocity.

3.3 Influence factors of transition velocities

3.3.1 Comparison of transition velocities based on H_{st}/D

Previous literature revealed that the transition velocities, U_S and U_C, are strongly depended on the ratio of the static bed height to the bed diameter (H_{st}/D) (Ellis *et al*. 2004 and Shaul *et al*. 2012). Ellis *et al*. (2004) found that U_C increases with H_{st}/D. The same result on the effect of bed diameter was also obtained by Du *et al*. (2005).

In this research, the effect of H_{st}/D on transition velocities (U_S and U_C) is investigated. A summary of experiment cases is given in Table 2. In addition, two different axial measured positions (ECT plane 1 and 2) are considered to study the effect of axial measured position. The results are shown in Fig. 12. As shown in Table 2, H_{st}/D of case 2 and case 6 are equal. The transition velocities of the two cases are almost equal in Fig. 12. It indicates that H_{st}/D as an influence factor on transition velocities is suitable for the riser in this study. In Fig. 12, the transition velocities (U_S and U_C) increase with H_{st}/D. This coincides with the previous study (Du *et al*. 2005, Ellis *et al*. 2004). As can be seen from Fig. 12, U_S is less affected by H_{st}/D than U_C. In general, the transition velocities of ECT plane 1 (upper plane) are smaller than those of ECT plane 2 (lower plane). The results indicate that with the increase of the gas velocity, the gas-solids flow at higher axial position of the riser reaches a different flow regime earlier, e.g. from bubbling regime to slugging regime. In other words, different flow regimes might exist along the riser. This was also confirmed by Rhodes *et al*. (1998) based on the analysis of gas-solids distributions both in the bottom and the top region in a fluidized bed riser.

<Table 2>

<Figure 12>

3.3.2 Comparison of transition velocities within the cross section

Bai *et al*. (1996a) reported that different local flow regimes might exist within the riser under the same superficial gas velocity. In this study, different local flow regimes in a same cross section are investigated

based on the ECT measurements. The pixels number inside the imaging area is 3001, which makes it possible to characterize the flow regimes locally. The results obtained from ECT plane 1 for the riser of 10 cm in diameter (H_{st} = 25 cm) are shown in Fig. 13. It shows the standard deviation and dominant frequency for four different radial positions. It can be seen that the standard deviation curves present a similar distribution, and the dominant frequency curves are approximately same. The transition velocities obtained from the standard deviation and dominant frequency analysis are marked with blue dotted lines in Fig. 13. It can be concluded that the transition velocities ($U_S^{"}$ and $U_C^{"}$) are nearly the same in different radial positions. The two transition velocities (0.8 m/s <$U_S^{"}$ <1.1 m/s and 2.0 m/s < $U_C^{"}$ < 2.5 m/s) are approximately equal to those (U_S = 1.1 m/s and U_C = 2.5 m/s) obtained from the average solids volume fraction in the cross section. The above results indicate that similar flow regimes might exist in different radial positions under the same operating condition.

<Figure 13>

4. Conclusions

In this research, the solids volume fractions measured by a twin-plane ECT sensor and pressure drop have been used to investigate the flow regimes in the bottom region of a CFB with different riser diameters. Time and frequency domain analysis are carried out to describe the dynamic behavior and define transition velocities. Three different flow regimes have been identified including bubbling, slugging and turbulent fluidization flow regime. The main conclusions are as follows.

(1) Gas-solids behavior in three flow regimes

In general, the average solids volume fraction within the measured cross section decreases with the superficial gas velocity. For the radial distribution, the solids volume fraction is low in the center and increases monotonically along the radial direction towards the wall region. The inhomogeneity of gas-solids flow in a cross section increases with the superficial gas velocity.

In the bubbling flow regime, bubble formation and breakup can be seen clearly. The average solids volume fraction in a cross section presents a periodic fluctuation with time. The solids volume fraction differences between different radial positions are relatively low. The standard deviation increases with the superficial gas velocity, but the dominant frequency decreases obviously.

In the slugging flow regime, the size and the number of bubble increase significantly. Thus both standard deviation and dominant frequency increase with the superficial gas velocity. The solids volume fraction decreases by almost 40 % in the center and almost 13 % near the wall. The periodicity of the average solids volume fraction in the cross section is not significant.

In the turbulent fluidization flow regime, gas-solids mixing increases due to the breakup of large bubble. The dominant frequency continues to increase while the standard deviation decreases from a maximum. The radial

profile of the solids volume fraction shows a smooth variation in the center and a steep variation near the wall.

(2) Bubble characteristics

Bubble diameter increases with the superficial gas velocity in the three flow regimes. In three risers, the bubble diameters are approximately equal under the same superficial gas velocity, because the distributor is made of a wire mesh.

The bubble rising velocity increases with the superficial gas velocity in the bubbling regime. In the slugging regime and turbulent fluidization regime, the bubble velocities become independent of the superficial gas velocity.

(3) Transition velocities (U_S and U_C)

In the bottom region of three risers, H_{st}/D as an influence factor on transition velocities is verified. Further study shows that transition velocities increase with H_{st}/D, and U_S is less affected by H_{st}/D than U_C. From the comparison studies on transition velocities in different measured positions, it can be concluded that the flow regimes at different axial heights are different. In contrast, the flow regimes within the cross section under the same operation condition might be similar to each other.

Acknowledgements

The authors are grateful to the support from the National Natural Science Foundation of China (No. 61320106004, No. 61374018) and Strategic Priority Research Program of the Chinese Academy of Sciences (No. XDA07030100).

Nomenclature

a	Area of each pixel (m^2)
A	Cross-sectional area of bed (m^2)
c_{xx}	Auto-correlation function (-)
C_H	Capacitance vector in close-packing (pf)
C_L	Capacitance vector in empty bed (pf)
C_M	Measurement capacitance vector (pf)
C_{xx}	Normalized auto-correlation function (-)
D	Inside diameter (m)
D_b	Bubble diameter (m)
g	Acceleration due to gravity (m/s^2)
G	Normalized grey level vector (-)

G^j	G obtained in *j-th* iteration (-)
h	Height of the bubble above the distributor (m)
H_{st}	Static bed height (m)
k	Δt number of time lag (-)
m_{max}	The maximum eigenvalue of S^TS(-)
M	Number of pixels in the imaging area (-)
N	ECT measurement number (-)
N_h	Number of holes in distributor (-)
r	Radial coordinate (m)
R	Riser radius (m)
S	Sensitivity matrix (-)
SD	Standard deviation (-)
Δt	Interval between ECT measurements (s)
u_λ	Identity vector (-)
U	Superficial gas velocity at the bottom of the riser (m/s)
U_C	Superficial gas velocity at the transition to turbulent fluidization regime (m/s)
U_{mf}	Critical fluidization velocity (m/s)
U_S	Superficial gas velocity at the transition to slugging regime (m/s)
Z	Axial height above the distributor (cm)

Greek symbols

α	Step length or gain factor (-)
β	Average solids volume fraction in cross section (-)
$\overline{\beta}$	Time-averaged β (-)
$\overline{\beta}_{center}$	Area-averaged $\overline{\beta}$ in the center (-)
$\overline{\beta}_{wall}$	Area-averaged $\overline{\beta}$ near the wall (-)
λ	Normalized capacitance vector (-)
θ	Close-packing volume fraction of experimental material (-)
τ	Relaxation factor (-)

References

Azzi, M., Turlier, P., Large, J.F. and Bernard, J.R. (1991), Use of a momentum probe and gamma-densitometry to study local properties of fast fluidized beds, Pergamon: Oxford, pp 189.

Bai, D., Shibuya, E., Nakagawa, N. and Kato, K. (1996a), Characterization of gas fluidization regimes using

pressure fluctuations, Powder Technology, 87, pp 105-111.

Bai, D., Shibuya, E., Masuda, Y., Nakagawa, N. and Kato, K. (1996b), Flow structure in a fast fluidized bed, Chemical Engineering Science, 51, pp 957-966.

Bhasker. C. (2002), Simulation of air flow in the typical boiler windbox segments, Advances in Engineering Software, 33, pp 793-804.

Chaplin, G., Pugsley, T., Lee, van der L., Kantzas, A. and Winters, C. (2005), The dynamic calibration of an electrical capacitance tomography sensor applied to the fluidized bed drying of pharmaceutical granule, Measurement Science and Technology, 16, pp 1281-1290.

Cui, H., Mostoufi, N. and Chaouki, J. (2001), Gas and solids between dynamic bubble and emulsion in gas-fluidized beds, Powder Technology, 120, pp 12-20.

Darton, R.C. (1977), Bubble growth due to coalescence in fluidised beds, Transactions of the Institution of Chemical Engineers, 55, pp 274-280.

Davidson, J.F. and Harrison, D. (1963), Fluidization particles, London: Cambridge University Press.

Davidson, J.F., Clift, R. and Harrison, D. (1985), Fluidization, Academic Press, London, 1985.

Depypere, F., Pieters, J.G. and Dewettinck, K. (2004), CFD analysis of air distribution in fluidised bed equipment, Powder Technology, 145, pp 176-189.

Du, B., Warsito, W. and Fan, L.S. (2005), ECT studies of gas-solid fluidized beds of different diameters, Industrial and Engineering Chemistry Research, 44, pp 5020-5030.

Dyakowski, T., Edwards, R.B., Xie, C.G. and Williams, R.A. (1997), Application of capacitance tomography to gas-solid flows, Chemical Engineering Science, 52, pp 2099-2110.

Ellis, N., Bi, H.T., Lim, C.J. and Grace, J.R. (2004), Hydrodynamics of turbulent fluidized beds of different diameters, Powder Technology, 141, pp 124-136.

Fan, L.T., Ho, T.C. and Walawender, W.P. (1983), Measurements of the rise velocities of bubbles, slugs and pressure waves in a gas-solid fluidized bed using pressure fluctuation signals, AIChE Journal, 29, pp 33-39.

Geldart, D. (1973), Types of gas fluidization, Powder Technology, 19, pp 285-292.

Hage, B., Werther, J., Narukawa, K. and Mori, S. (1996), Capacitance Probe measurement technique for local particle volume concentration in Circulating Fluidized Bed Combustors, Journal of Chemical Engineering of Japan, 29, pp 594-602.

Hilligardt, K. and Werther, J. (1986), Local bubble gas hold-up and expansion of gas/solid fluidized beds, German Chemical Engineering, 9, pp 215-221.

Johnsson, F., Zijerveld, R.C., Schouten, J.C., Van den Bleek, C.M. and Leckner, B. (2000), Characterization of fluidization regimes by time-series analysis of pressure fluctuations, International Journal of Multiphase Flow, 26, pp 663-715.

Karimipour, S. and Pugsley, T. (2011), A critical evaluation of literature correlations for predicting bubble size and velocity in gas-solid fluidized beds, Powder Technology, 205, pp 1-14.

Kim, S.W., Hirbas, G., Bi, H.T., Lim C.J. and Grace J.R. (2004), Flow behavior and regime transition in a high-density circulating fluidized bed riser, Chemical Engineering Science, 59, pp 3955-3963.

Kim, Y.S., Lee, S.H., Ijaz, U.Z., Kim, K.Y. and Choi, B.Y. (2007), Sensitivity map generation in electrical capacitance tomography using mixed normalization models, Measurement Science and Technology, 18, pp 2092-2102.

Lehner, P. and Wirth, K.E. (1999), Characterization of the flow pattern in a downer reactor, Chemical Engineering Science, 54, pp 5471-5483.

Liu, S., Chen, Q., Wang, H.G., Ismail, I. and Yang, W.Q. (2005), Electrical capacitance tomography for gas-solids flow measurement for circulating fluidized beds, Flow Measurement and Instrumentation, 16, pp 135-134.

Liu, S., Fu, L. and Yang, W.Q. (1999), Optimization of an iterative image reconstruction algorithm for electrical capacitance tomography, Measurement Science and Technology, 10, L37-L39.

Makkawi, Y.T. and Wright, P.C. (2002), Fluidization regimes in a conventional fluidized bed characterized by means of electrical capacitance tomography, Chemical Engineering Science, 57, pp 2411-2437.

Malcus, S., Chaplin, G. and Pugsley, T. (2000), The hydrodynamics of the high-density bottom zone in a CFB riser analyzed by means of electrical capacitance tomography (ECT), Chemical Engineering Science, 55, pp 4129-4138.

Monazam, E.R., Shadle, L.J. Mei, J.S. and Spenik, J. (2005), Identification and characteristics of different flow regimes in a circulating fluidized bed, Powder Technology, 155, pp 17-25.

Piskova, E. and Mörl, L. (2008), Characterization of spouted bed regimes using pressure fluctuation signals, Chemical Engineering Science, 63, pp 2307-2316.

Rhodes, M.J., Sollaart, M. and Wang, X.S. (1998), Flow structure in a fast fluid bed, Powder Technology, 99, pp 194-200.

Shaul, S., Rabinovich, E. and Kalman, H. (2012), Generalized flow regime diagram of fluidized beds based on the height to bed diameter ratio, Powder Technology, 228, pp 264-271.

Srivastava, A., Agrawal, K., Sundaresan, S., Reddy Karri, S.B. and Knowlton, T.M. (1998), Dynamics of gas-particle flow in circulating fluidized beds, Powder Technology, 100, pp 173-182.

Svensson, A., Johnsson, F. and Leckner, B. (1996), Fluidization regimes in non-slugging fluidized beds: the influence of pressure drop across the air distributor, Powder Technology, 86, pp 299-312.

van Wachem, B.G.M., Schouten, J.C., Krishna, R. and van den Bleek, C.M. (1998), Eulerian simulations of bubbling behaviour in gas-solid fluidised beds, Computers & Chemical Engineering, 22, pp S299-S306.

Wang, H.G., Senior, P.R., Mann, R. and Yang, W.Q. (2009), Online measurement and control of solids moisture in fluidised bed dryers. Chemical Engineering Science, 64, 2893-2902.

Wang, H.G., Yang, W.Q., Dyakowski, T. and Liu, S. (2006), Study of bubbling and slugging fluidized beds by simulation and ECT. AIChE Journal, 52, 3078-3087.

Wang, H.G. and Yang, W.Q. (2010), Measurement of fluidised bed dryer by different frequency and different normalisation methods with electrical capacitance tomography, Powder Technology, 199, pp 60-69.

Wang, H.G. and Yang, W.Q. (2011), Scale up of an electrical capacitance tomography sensor for imaging pharmaceutical fluidized beds and validation by computational fluid dynamics, Measurement Science and Technology, 22, no.104015.

Wang, S.J., Dyakowski, T., Xie, C.G., Williams, R.A. and Beck, M.S. (1995), Real time capacitance imaging of bubble formation at the distributor of a fluidized bed, The Chemical Engineering Journal and The Biochemical Engineering Journal, 56, pp 95-100.

Wiesendorf, V. and Werther, J. (2000), Capacitance probes for solids volume concentration and velocity measurements in industrial fluidized bed reactors, Powder Technology, 110, pp 143-157.

Yang, W.Q., Spink, D.M., York, T.A. and McCann, H. (1999), An image-reconstruction algorithm based on Landweber's iteration method for electrical-capacitance tomography, Measurement Science and Technology, 10, pp 1065-1069.

Yang, W.Q. and York, T.A., (1999), New AC-based capacitance tomography system, IEE Proc.-Sci. Meas. Technol., 146, pp 47-53.

Zijerveld, R.C., Johnsson, F., Marzocchella, A., Schouten, J.C. and van der Bleek, C.M. (1998), Fluidization regimes and transitions from fixed bed to dilute transport flow, Powder Technology, 95, pp 185-204.

Figures:

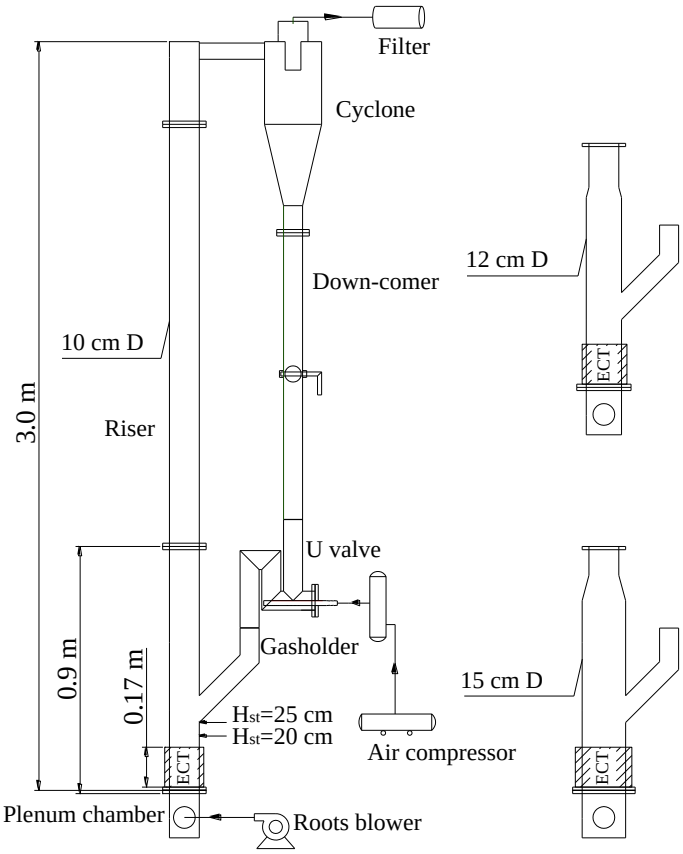

Figure 1. Circulating fluidized bed.

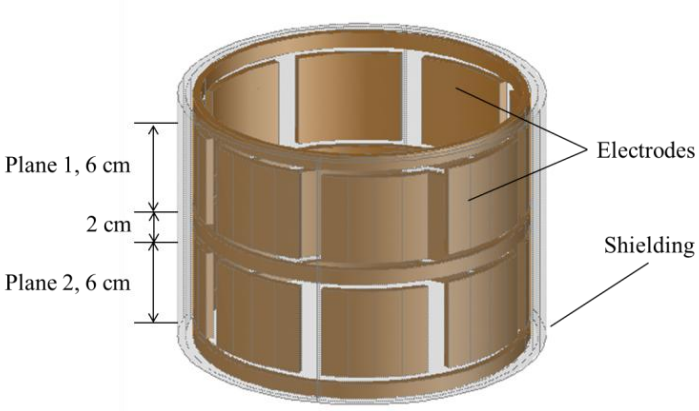

Figure 2. ECT sensor.

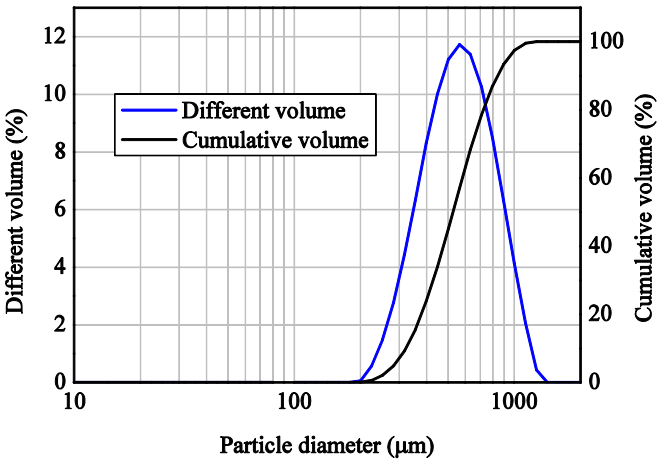

Figure 3. Particle size distribution

(a)

(b)

(c)

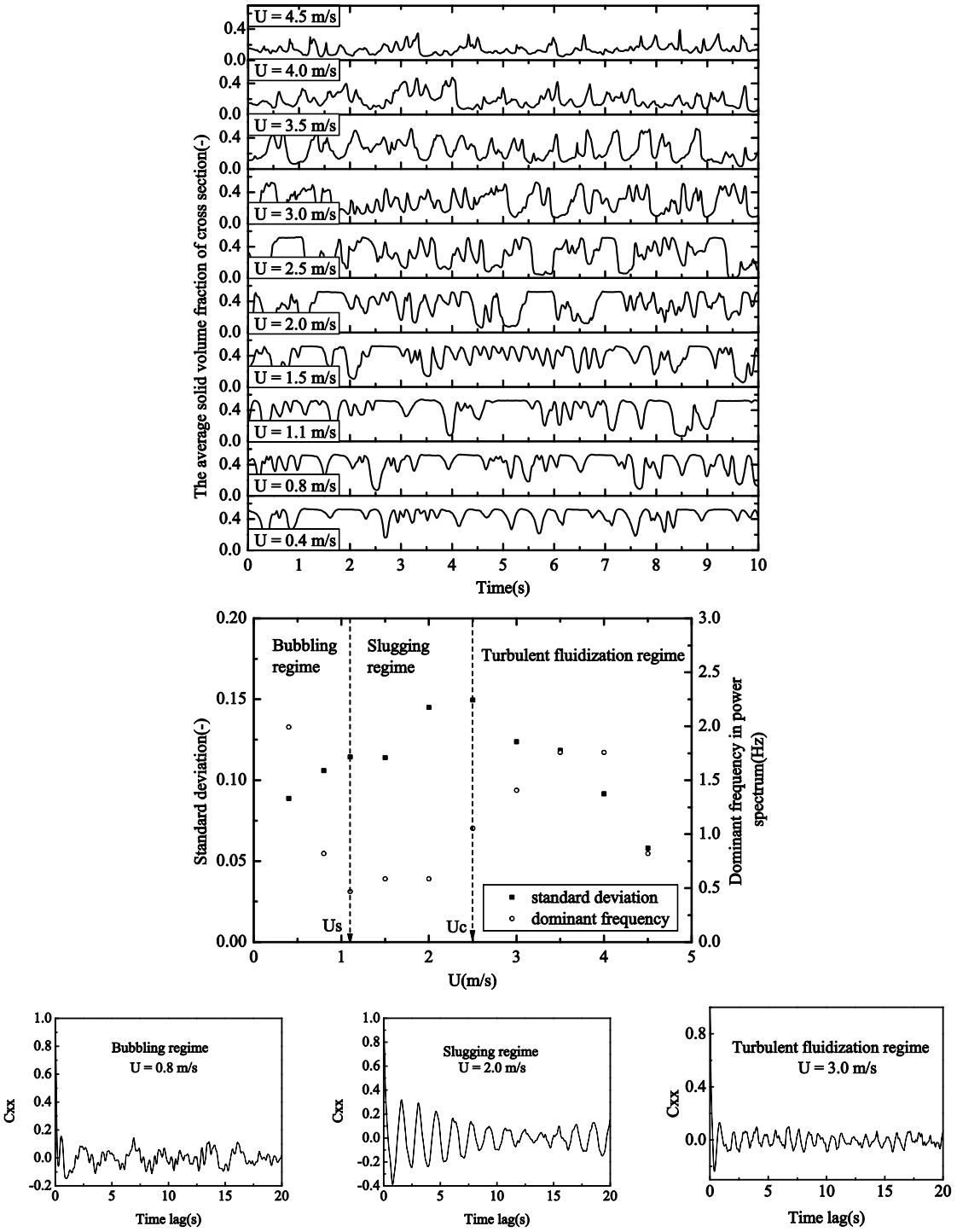

Figure 4. Time domain analysis on the solids volume fraction fluctuations for different superficial gas velocity. (a) Solids volume fraction fluctuations at different superficial gas velocity. (b) Standard deviation and dominant frequency in power spectrum of average solids volume fraction. (c) Auto-correlation coefficient.

(a)

(b)

(c)

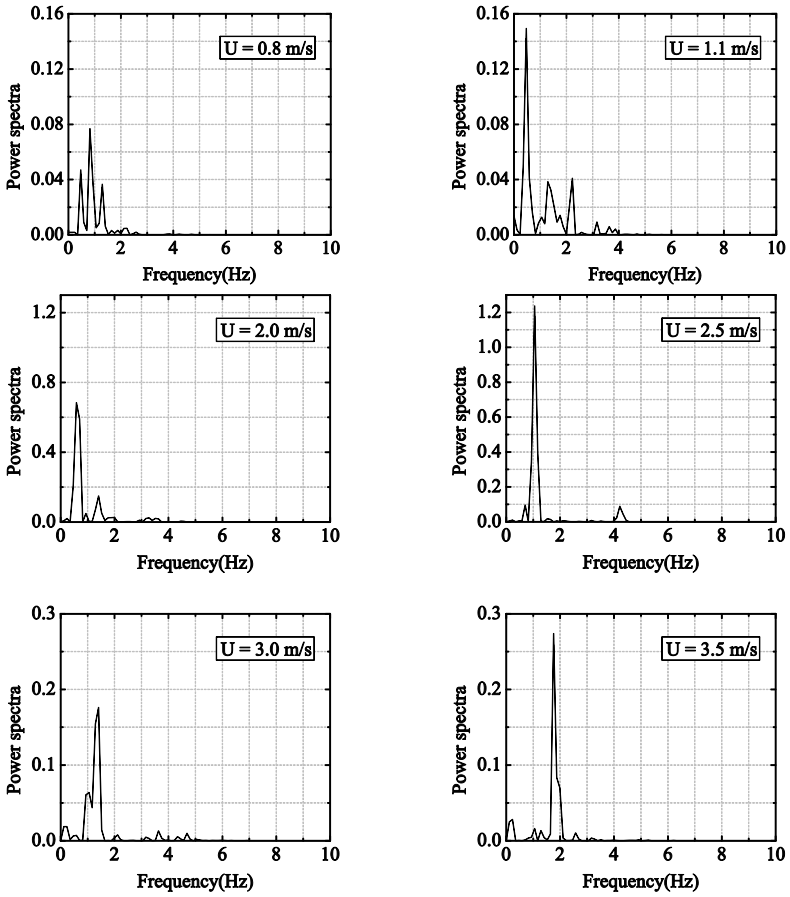

Figure 5. Power spectra of average solids volume fraction in cross section. (a) Bubbling regime. (b) Slugging regime. (c) Turbulent fluidization regime.

(a)

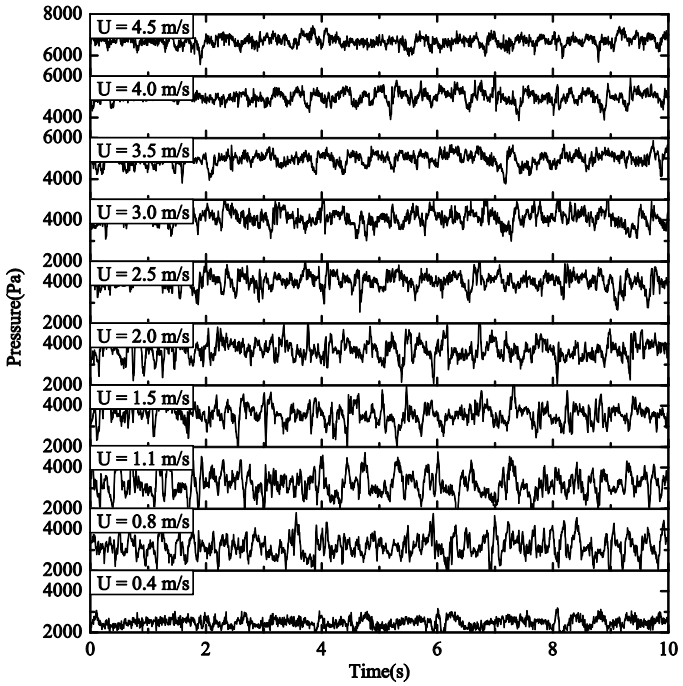

(b)

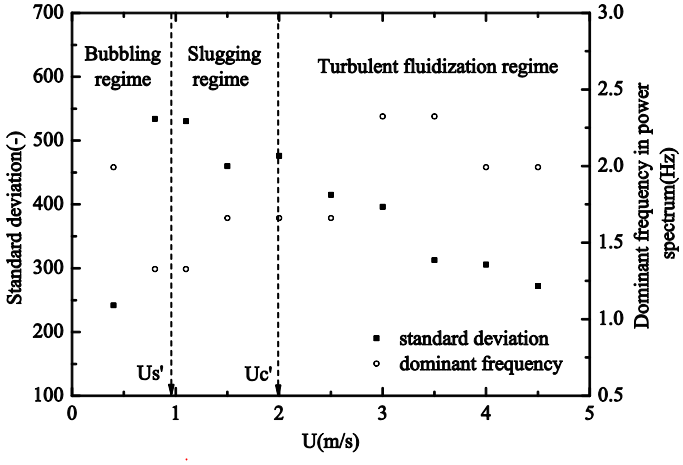

(c)

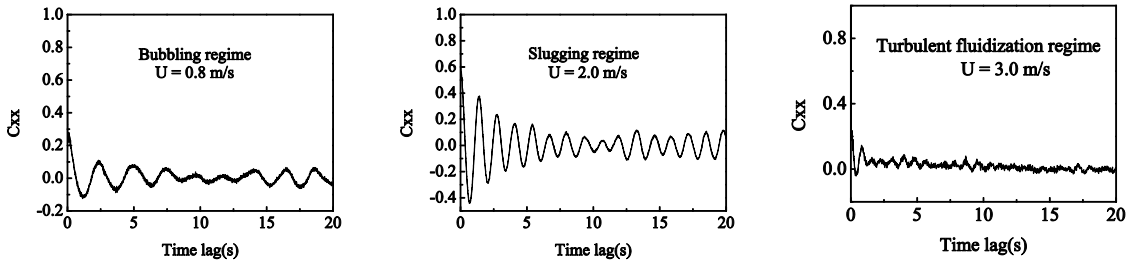

Figure 6. Time domain analysis on the differential pressure fluctuations for different superficial gas velocity. (a) Pressure fraction fluctuations at different superficial gas velocity. (b) Standard deviation and dominant frequency in power spectrum of pressure fluctuations. (c) Auto-correlation coefficient.

(a)

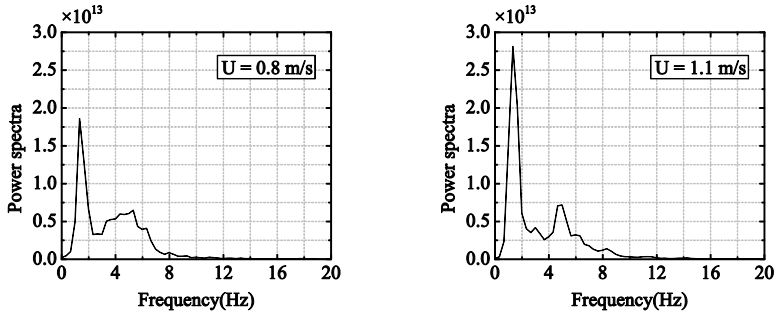

(b)

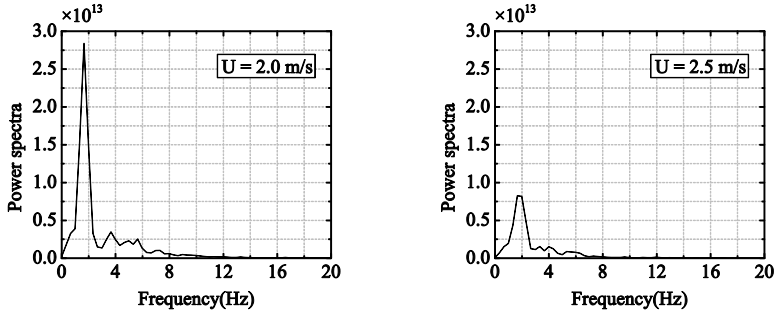

(c)

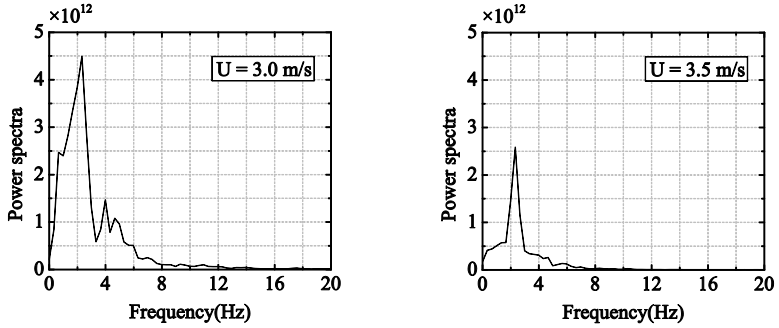

Figure 7. Power spectra of differential pressure fluctuations. (a) Bubbling regime. (b) Slugging regime. (c) Turbulent fluidization regime.

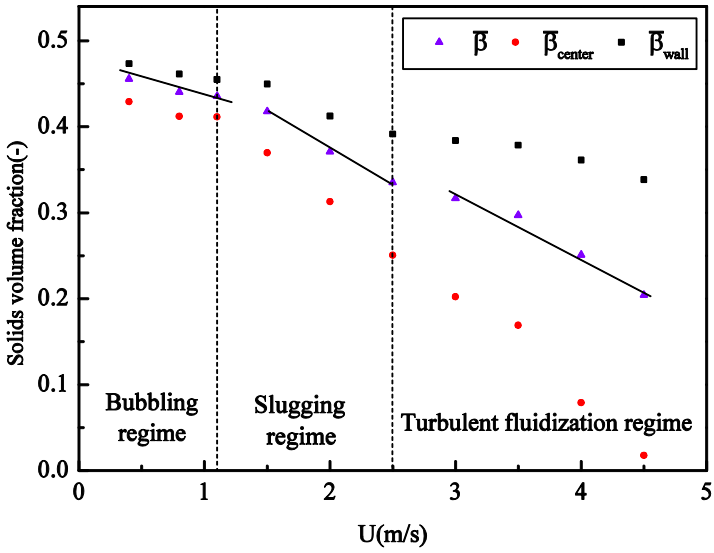

(a)

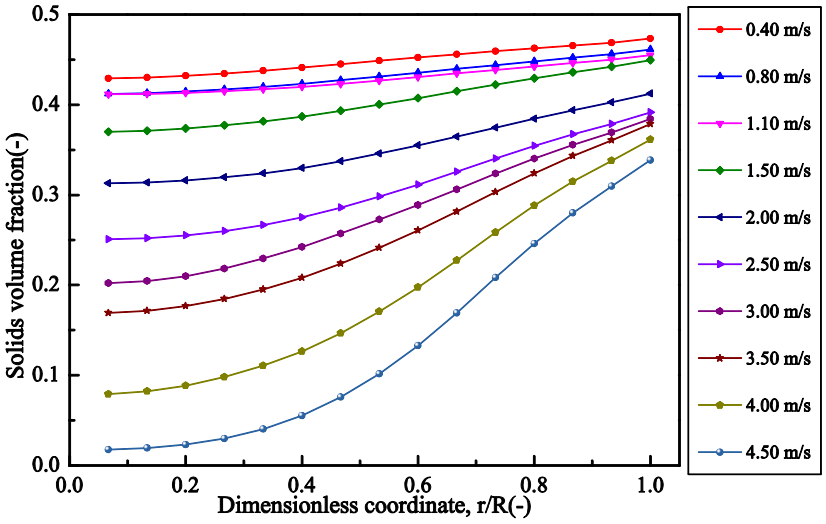

(b)

Figure 8. Solids volume fraction distribution. (a) Solids volume fraction averaged in time as a function of superficial gas velocity. (b) Radial profiles of solids volume fraction.

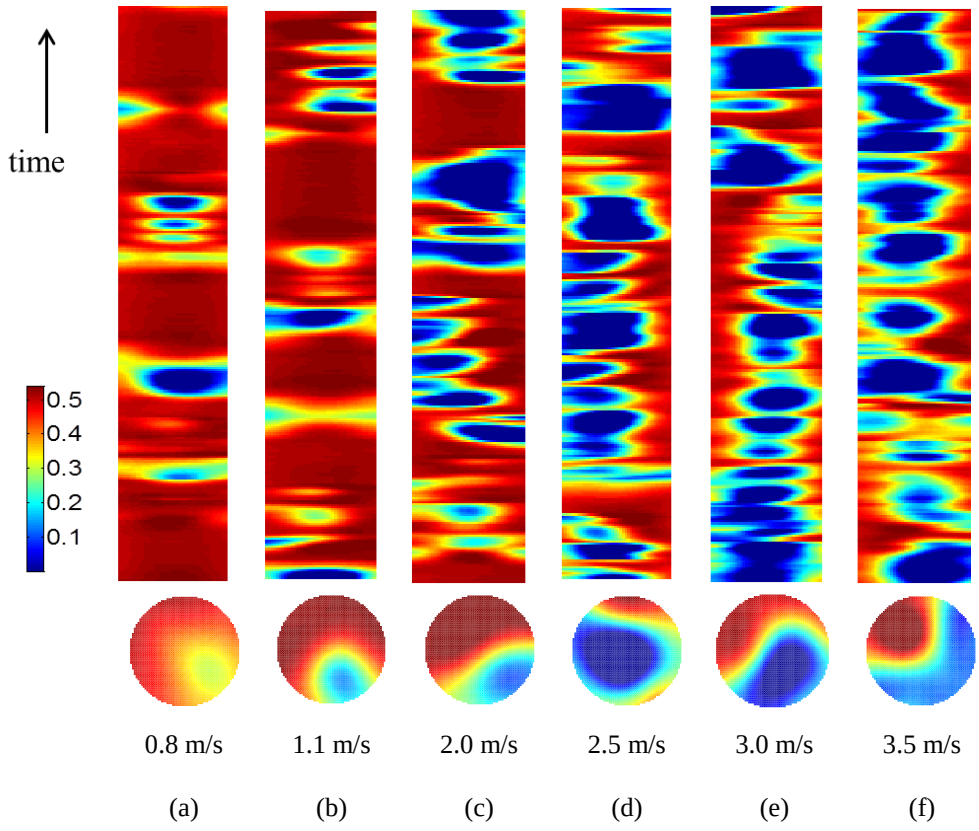

Figure 9. Quasi-three-dimensional solids volume fraction distribution.

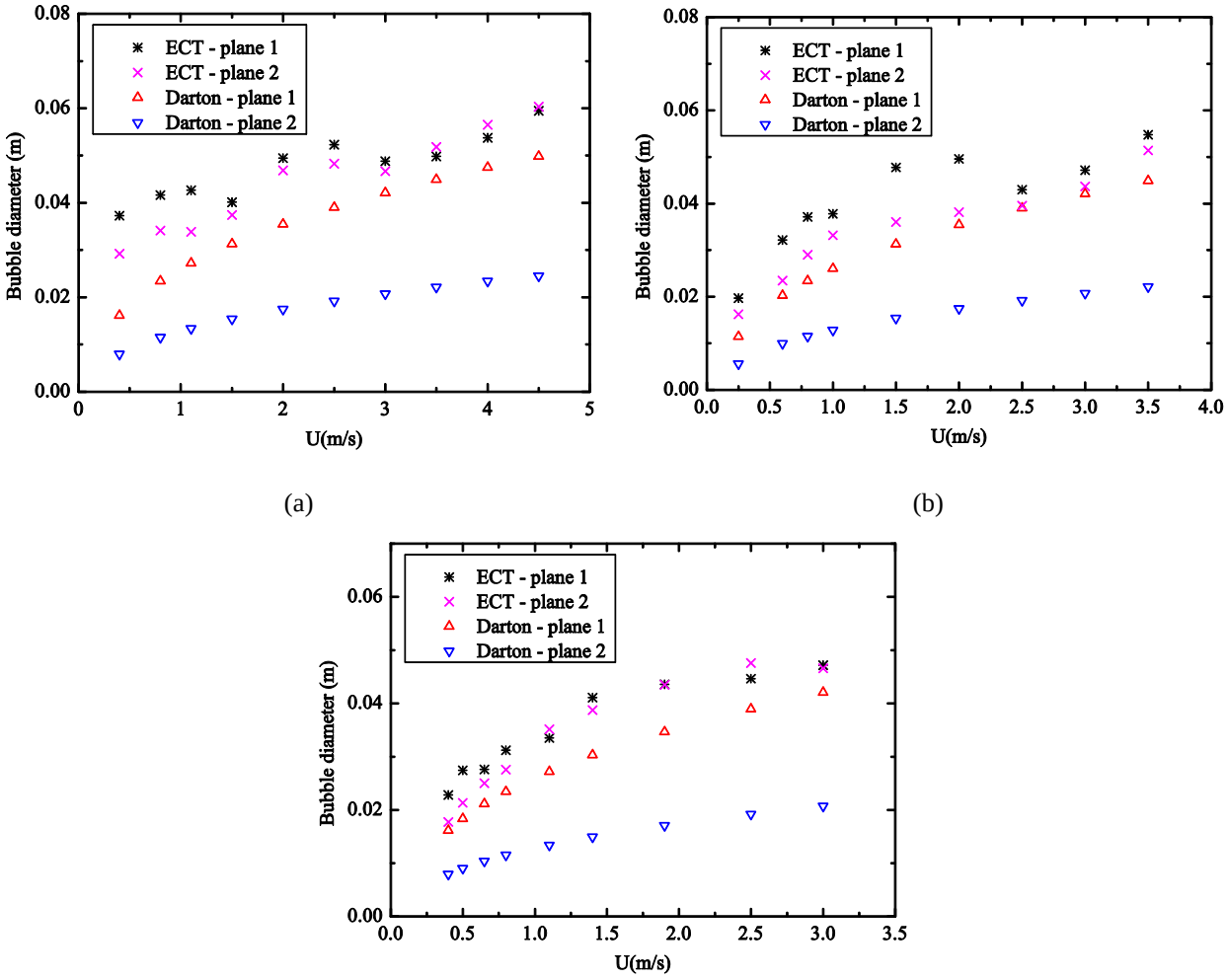

Figure 10. Bubble diameter for various gas superficial velocities. (a) 10 cm D. (b) 12 cm D. (c) 15 cm D.

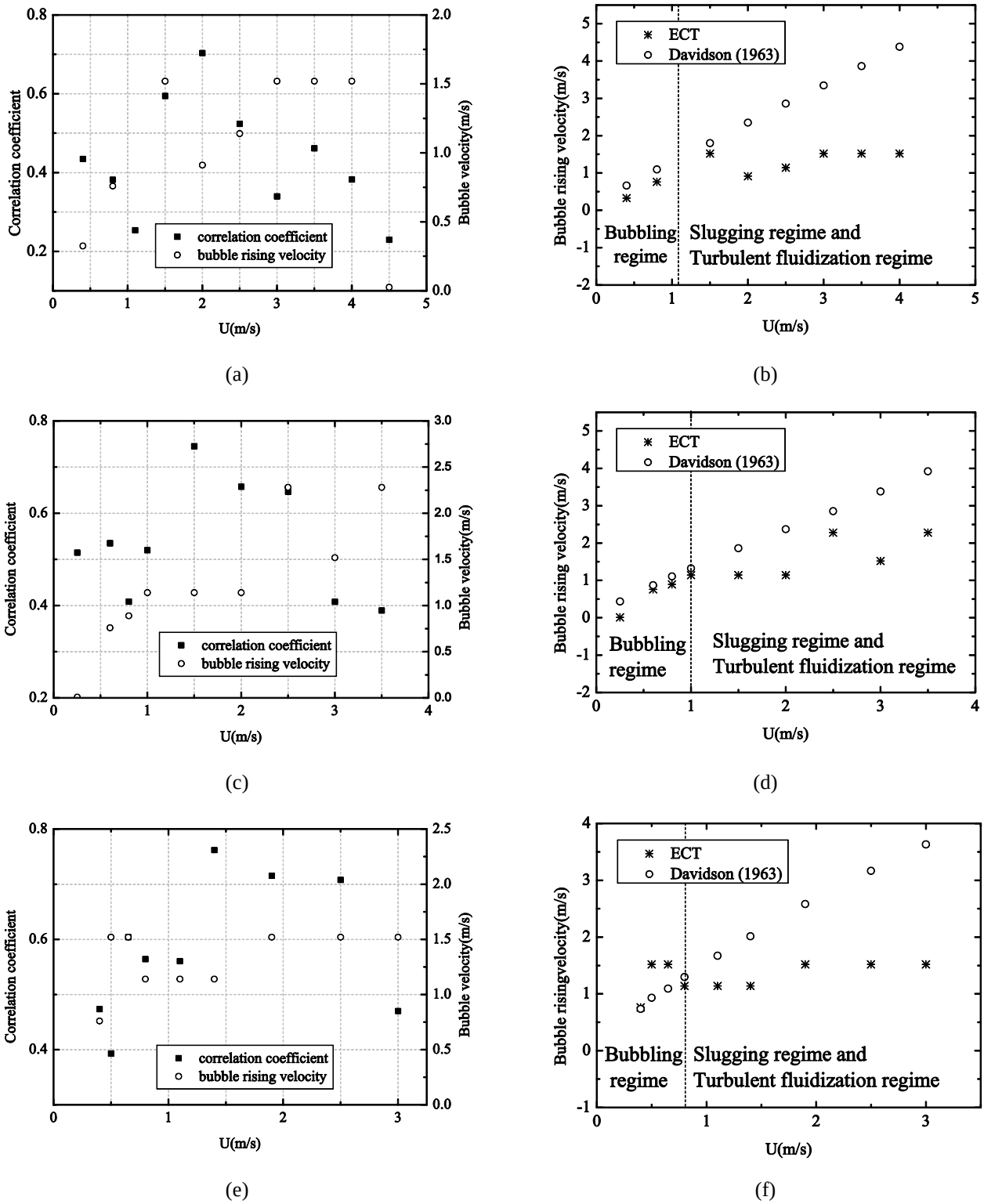

Figure 11. The results of correlation analysis and bubble rising velocity. (a) Correlation analysis for 10 cm D. (b) Bubble rising velocity for 10 cm D. (c) Correlation analysis for 12 cm D. (d) Bubble rising velocity for 12 cm D. (e) Correlation analysis for 15 cm D. (f) Bubble rising velocity for 15 cm D.

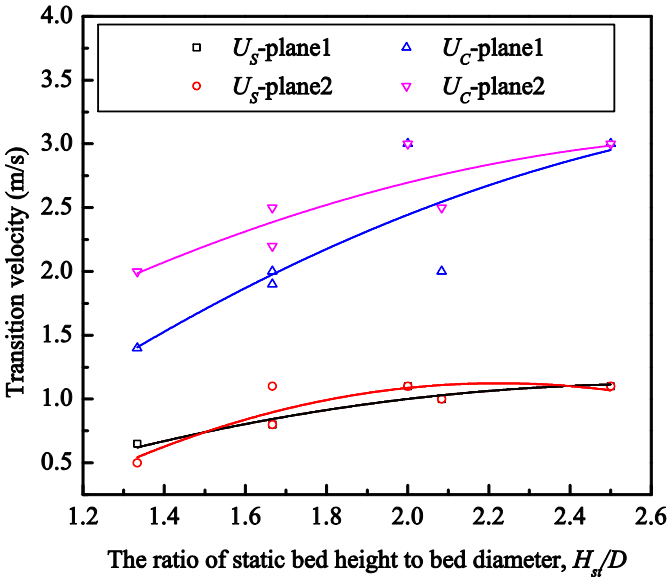

Figure 12. Transition velocity via the ratio of the static bed height to bed diameter.

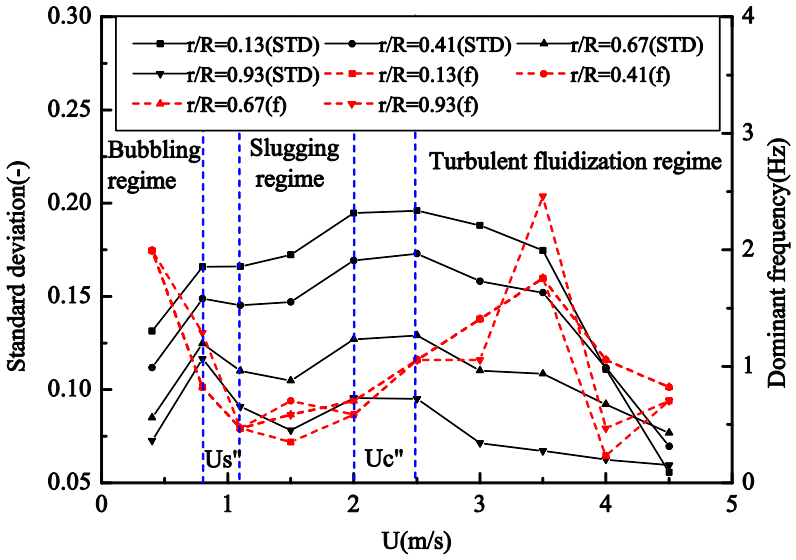

Figure 13. Radial standard deviation and dominant frequency against superficial gas velocity.

Tables:

Table 1 Summary of the experimental operation conditions

Experimental unit	Operating conditions
Riser	D = 10 cm, 12 cm, 15 cm, height = 3.0 m
Distributor	Material: wire gauze, 100 mesh, Z = 0
Fluidizing gas	Air at ambient conditions
Superficial gas velocity	0.4-4.5 m/s for 10 cm D., 0.25-3.5 m/s for 12 cm D., 0.2-3.0m/s for 15 cm D.
Particle	Material: sand, mean diameter = 469 μm, bulk density = 1608 kg/m^3
Static bed height	20 cm, 25 cm
ECT system	Plane 1: Z = 2.5-8.5 cm, plane 2: Z = 10.5-16.5 cm, eight electrodes per plane
DP transducer	Z = 2.5-16.5 cm

* Z means the axial height above the distributor

Table 2 Summary of experiment cases (H_{st}/D)

	Case 1	Case 2	Case 3	Case 4	Case 5	Case 6
H_{st}(cm)	20	20	20	25	25	25
D(cm)	10	12	15	10	12	15
H_{st}/D	2	1.67	1.33	2.5	2.08	1.67

Submitted to *Chemical Engineering Science* (Revised Version 25 Apr. 2014)

Investigation of flow hydrodynamics and regime transition in a gas-solids fluidized bed with different riser diameters

Guizhi Qiu[1,2], Jiamin Ye [1], Haigang Wang [1*], Wuqiang Yang[3]

[1.] Institute of Engineering Thermophysics, Chinese Academy of Sciences, PO Box 2706, Beijing 100190, China

[2.] University of Chinese Academy of Sciences, PO Box 2706, Beijing 100190, China

[3.] School of Electrical and Electronic Engineering, The University of Manchester, Sackville Street, Manchester M13 9PL, UK

Abstract: It is important to understand the flow hydrodynamics behavior of a circulating fluidized bed (CFB) reactor for efficient operation. The objective of this research is to identify and characterize the flow regimes in a fluidized bed with different riser diameters. For this purpose, electrical capacitance tomography (ECT) combined with pressure measurement has been used to investigate the flow characteristics and flow regime transitions. Experiment was carried out in a cold gas-solids fluidized bed to investigate the flow regimes and the transition velocities. Three risers of different diameter, 10, 12 and 15 cm, are designed and used for comparison. A twin-plane ECT sensor and a differential pressure transducer are used to obtain the solids volume fraction and differential pressure in the bottom region. Different flow regimes including bubbling, slugging and turbulent flow regime were formed with two distinct transition velocities. The flow characteristics are investigated in terms of solids volume fraction, bubble diameter and bubble rising velocity. The transition velocities are compared based on the ratio of the static bed height to bed diameter (H_{st}/D) and the measured position (i.e. the axial position and radial position).

Keywords: Flow regime, Electrical capacitance tomography, Differential pressure, Solids volume fraction, Bubble characteristic, Transition velocity

1. Introduction

Circulating fluidized bed (CFB) reactors have been widely used in industrial processes, including coal combustion, biomass pyrolysis, coal gasification, and catalytic cracking. It provides good gas-solids mixing and excellent heat and mass transfer properties. The reactor performance is significantly depended on the

[*] Correspondence author, Tel.: 0086-10-82543140, E-mail: wanghaig@hotmail.com (H.G. Wang)

dynamics properties of the gas-solids two-phase flow system (Davidson *et al*. 1985). According to the characteristics of gas-solid fluctuations, the fluidization behavior has been widely classified into several flow regimes, including the bubbling, slugging, turbulent and fast fluidization flow regime (Johnsson *et al*. 2000, Svensson *et al*. 1996, Zijerveld *et al*. 1998).

However, due to the change in dimensions and geometrical parameters, i.e. CFB riser's chamber shape and diameter, the flow hydrodynamics and regime transition will be different from each other which results in the change of heat and mass transfer characteristics (Kim *et al*. 2004). Furthermore, the flow regime transition is strongly depended on the diameter of riser and operating condition (Shaul *et al*. 2012). For process optimization and scale-up purposes, it is necessary to investigate the flow behavior and different flow regime transitions in a fluidized bed with different riser diameters.

In general, the flow regimes can be identified by standard deviation and frequency spectrum of measured parameters, such as pressure drop (Bai *et al*. 1996a, Johnsson *et al*. 2000, Monazam *et al*. 2005, Piskova and Mörl 2008). Fan *et al*. (1983) characterized the flow regimes by measuring the bubble rising velocity using pressure fluctuation signals. The solids volume fraction has also been widely used to analyze the flow regime and it can be measured by intrusive techniques such as a momentum probe (Azzi *et al*. 1991, Bai *et al*. 1996b), a capacitance probe (Hage *et al*. 1996, Wiesendorf and Werther 2000) and an optical fiber probe (Cui *et al*. 2001, Ellis *et al*. 2004). However, it is difficult to measure the flow variations in a cross section simultaneously which is a key to optimize the process operation in a fluidized bed, especially in a large-scale fluidized bed (Wang *et al*. 2006). As a reliable non-invasive technique, electrical capacitance tomography (ECT) can present the cross-sectional images for measuring the solids volume fraction and analyzing the flow behavior (Dyakowski *et al*. 1997, Lehner and Wirth 1999, Malcus *et al*. 2000). Numerous research studies have been reported on the analysis of flow regime characteristics in fluidized beds based on ECT measurements (Du *et al*. 2005, Malcus *et al*. 2000, Makkawi and Wright 2002, Srivastava *et al*. 1998, Wang *et al*. 1995). Du *et al*. (2005) studied the bubble characteristics by the quasi-three dimensional flow structures of a gas-solid fluidized bed using ECT. Johnsson *et al.* (2000) and Makkawi *et al.* (2002) studied the identification of flow regimes and the results indicated that the dominant frequency reached a minimum at the transition point from bubbling to slugging flow regime, while the standard deviation reached a maximum at the transition point from slugging to turbulent flow regime.

However, most of the previous researches are focused on the flow hydrodynamics characteristics and little attention has been paid to the factor which influences the transition velocity. Bai *et al.* (1996a) pointed out that the transition velocity was influenced by many factors including measured position and bed geometries. Rhodes *et al*. (1998) confirmed that different flow regimes existed along the riser based on the analysis of the gas-solids flow behavior both in the bottom and the top region. Du *et al.* (2005) studied the effect of the bed diameter on the transition velocity from slugging to turbulent flow regime. It indicated that the transition velocity decreases with the increase of bed diameter. Ellis *et al.* (2004) and Shaul *et al.* (2012) generalized the transition velocity based on the height to bed diameter ratio. Ellis (2004) found that the transition velocity from slugging to turbulent fluidization flow regime increased with the ratio of bed height to bed diameter.

Although considerable research efforts have been made in the analysis of fluidized bed hydrodynamic, a systematic study on the gas-solids flow dynamic characteristics, especially the flow regime transition, is still necessary to optimize the design and process operation for a circulating fluidized bed with different riser diameters. In this research, the gas-solids hydrodynamics flow structure in the bottom of CFB risers with different diameter has been studied based on ECT measurements combined with differential pressure fluctuations analysis. The ultimate objectives of this research are: (1) to understand the flow behavior in a gas-solids fluidized bed with different riser diameters based on key process parameters, (2) to investigate the flow regime characteristics, including the solids volume fraction, bubble diameter and bubble rising velocity, and (3) to study the effect of riser diameter, static bed height and measured position on the transition velocity.

2. Experiment

2.1 Experimental setup

Fig. 1 shows the experimental setup of a gas-solids circulating fluidized bed, which consists of a riser of 3.0 m in height, a cyclone and a non-mechanical U-valve. The entire system is made of cast acrylic except for a steel cyclone separator. The bottom of the riser is designed with three different inside diameters (10, 12 and 15 cm). Airflow at ambient temperature is introduced to the riser to fluidize the particles through a trefoil Roots blower and a wire gauze air distributor. A plenum chamber is designed below the air distributor to provide a uniform air distribution over the whole cross-section of the riser and to maintain a turbulence-free airflow (Depypere *et al*. 2004). The Airflow is manually controlled by using two bypass valves located downstream of the blower assisted by operating frequency fine-tuning and the percentage deviation of airflow was less than 5 %. The pipe from the Roots blower to the plenum chamber, with a length of about 20 m, can weaken the influence of airflow fluctuation. Therefore, the effect of the airflow fluctuation on the gas-solids flow hydrodynamics in the riser can be neglected. The superficial gas velocity is measured by a turbine flow meter and adjusted to correct the change in temperature and pressure in the plenum chamber. Particles are carried upwards in the riser and exit from the top through a right-angled tube connected to a cyclone where particles are separated from the gas phase. Particles separated by the cyclone are fed back to the bottom of the riser through the U-valve as shown in Fig. 1.

<Figure 1>

2.2. ECT sensor design

Fig. 2 shows the structure of the ECT sensor used in this research. It consists of two planes (plane 1 and plane 2). Each plane has eight electrodes made of self-adhesive copper tape. The electrodes are stuck to the outside wall of the riser and covered by shielding copper to eliminate external interference. The riser wall is made of cast acrylic with thickness of 0.5 cm. Chaplin *et al*. (2005) indicated that the possible influence of the permittivity of the acrylic cone wall is negligible. In addition, the wall effect on the capacitance has been compensated in the low and high calibrations which are used to normalize the measured capacitances (Yang

and York 1999). The mid-positions of plane 1 and plane 2 locate at 13.5 cm and 5.5 cm above the air distributor respectively. The length of the electrodes is 6 cm. The widths of the electrodes are 3.5, 4.0 and 5.0 cm for the three risers with different diameter 10, 12 and 15 cm, respectively. An AC-based electrical capacitance tomography (AC-ECT) system with 16 channels (Yang and York 1999) is employed for the experiments. The DC power supply provides the earth or ground for shielding the electrodes to eliminate the noise effect from environment. The AC-ECT system used in this research has a high signal-to-noise ratio (SNR) which used to indicate the signals quality (Yang and York 1999). Moreover, low-pass-filter is used to eliminate the noise effect on the signals to improve the image quality (Wang *et al*. 2009). The image acquisition rate for each plan of the twin-plane ECT sensor is 60 frames per second and the number of data acquisition is set to be 10,000 for each measurement.

<Figure 2>

2.3. Image reconstruction

An optimized iterative algorithm based on the Landweber method is used for image reconstruction (Liu *et al*. 1999). The reconstructed image is divided into 64×64 grids, which results in 3001 effective pixels in the circular cross section or measurement area in the riser. The optimized iterative algorithm is expressed as

$$G^{j+1} = G^{j} \cdot (1.0 + \tau) + \alpha \cdot S^{T} \cdot (\lambda - S \cdot G^{j}) \cdot (1 - \tau) \tag{1}$$

where G is the normalized permittivity distribution, which is often called grey level vector in image reconstruction to indicate the percentage occupied by particles. G^j is G obtained in *j-th* iteration. G^0, the first matrix of G^j, is calculated by Linear back projection (LBP) and expressed as

$$G^{0} = \frac{S^{T}\lambda}{S^{T}u_{\lambda}} \tag{2}$$

where S is the sensitivity matrix for the ECT sensor, u_λ is an identity vector, λ is the normalized capacitance vector calculated by Eq. 4. The detail for the calculation of sensitivity matrix of S is given in reference (Kim *et al*. 2007).

In Eq. 1, τ is a relaxation factor. There are no general rules for choosing the best value for the relaxation factor. The optimum value depends on a number of factors, e.g. the nature of the problem, the number of grid points, the grid spacing, and the iteration procedure used (Wang and Yang 2010). In this paper, the value of τ is 0.005.

In Eq. 1, α is a step length or gain factor, which a suitable size of the gain factor can be estimated to be (Yang *et al*. 1999)

$$\alpha = 2/m_{\max} \tag{3}$$

where m_{max} is the maximum eigenvalue of S^TS.

In Eq. 2, λ is calculated by

$$\lambda = \frac{C_M - C_L}{C_H - C_L} \tag{4}$$

where C_M is the measurement capacitance vector, C_H and C_L represent the capacitance vector measured in close-packing and empty bed respectively. To normalize the measurement capacitance of C_M by Eq. 4, high and low calibrations need to be performed to get the capacitance data of C_H and C_L before the experiment. In this research, the high calibration is done by filling the ECT sensor with sands used in the experiment and the measured capacitance is saved as C_H. And the low calibration is done by empting the ECT sensor with air and the measured capacitance is saved as C_L. A detailed calibration procedure is given in reference (Yang and York 1999).

2.4. Pressure acquisition

A differential pressure transducer (Setra 268110KLD11FF2NN) is used to measure the pressure drop of the corresponding zone of the twin-plane ECT sensor. Two pressure taps are installed along the riser wall located at 2.5 cm and 16.5 cm above the air distributor and connected to the differential pressure transducer, which is interfaced with a PC for data acquisition. In this work, the data acquisition rate is set as 170 samples per second and the data acquisition time is100 seconds.

2.5. Experiment conditions and materials

The particles used in this study are sands (mixture of Group B particles, according to Geldart classification (Geldart 1973)) with a mean diameter of 469 μm and the particle size distribution is shown in Fig. 3. The bulk density is 1608 kg/m^3 and the close-packing volume fraction is 0.54. Experiments are carried out with two static bed heights (H_{st} = 20 cm and 25 cm), which are marked in Fig. 1. The detailed experiment conditions are summarized in Table 1.

<Figure 3>

<Table 1>

3. Results and discussion

3.1 Flow regime identification

3.1.1 Time and frequency domain analysis on solids volume fraction

Time and frequency domain analysis are the most common approach to describing the dynamic behavior in a gas-solids flow system and defining the flow regime transition (Makkawi and Wright 2002, Piskova and Mörl 2008). In this research, the solids volume fraction is analyzed in terms of standard deviation, auto-correlation function and power spectrum.

The area-averaged solids volume fraction in a cross section, β, is calculated by

$$\beta = \vartheta \cdot \overline{G} = \vartheta \cdot \frac{\sum_{i=1}^{M} G_i \cdot a_i}{\sum_{i=1}^{M} a_i} \tag{5}$$

where θ is the close-packing volume fraction of experimental material, which is 0.54 in this research, G is the normalized permittivity distribution calculated by Eq. 1, a is the effective pixel area and M is the effective pixel number inside the circular imaging area, which is 3001.

The standard deviation (SD) of β is defined as

$$\mathrm{SD} = \sqrt{\frac{1}{N-1}\sum_{i=1}^{N}(\beta_i - \overline{\beta})^2} \tag{6}$$

where, β_i is a time series of β, and $\overline{\beta}$ is the time-averaged of β_i, N is the total number of measurements, which is 10,000.

To quantify the temporal patterns, the auto-correlation function between two points separated by a time lag, k times Δt, is calculated by (Johnsson *et al*., 2000)

$$c_{xx}(k) = \sum_{n=0}^{N-|k|-1}(\beta_i - \overline{\beta})(\beta_{i-k} - \overline{\beta}) \tag{7}$$

The auto-correlation function is normalized with the value at zero lag, $c_{xx}(0)$, thus

$$C_{xx}(k) = \frac{c_{xx}(k)}{c_{xx}(0)} \tag{8}$$

i.e. $-1 \leq C_{xx} \leq 1$.

The results obtained from the ECT plane 1 for the riser of 10 cm in diameter (H_{st} = 25 cm) are shown in Fig. 4, including the time domain analysis on area-averaged solids volume fraction, β. Three different flow regimes can be identified from Fig. 4: (1) bubbling flow regime, (2) slugging flow regime and (3) turbulent fluidization flow regime. Fig. 4 (a) shows the average solids volume fraction fluctuations under different superficial gas velocities. It can be found that β varies (significantly different in amplitude and frequency) with time periodically for each superficial gas velocity. Fig. 4 (b) shows the standard deviation and the dominant frequency, which is obtained by power spectra analysis as shown in Fig. 5, against the superficial gas velocity. With a low superficial gas velocity, the standard deviation increases with the superficial gas velocity and reaches a maximum at 2.5 m/s. This peak corresponds to the well-known transition velocity called $U_{C,}$ which is defined as the mark for the onset of turbulent fluidization regime (Bai *et al*. 1996b). The fluctuation of gas-solids flow reaches a maximum at U_C. With the further increase in superficial gas velocity, the standard deviation decreases dramatically due to the breakup of large bubbles.

Referencing the dominant frequency distribution as shown in Fig. 4 (b), it can be found that the fluctuation starts with a high frequency (2.0 Hz) and then decreases to a minimum (0.5 Hz) at U = 1.1 m/s, which marks the end of bubbling flow regime. This velocity is defined as the transition velocity from the bubbling to slugging flow regime, U_S. Another small peak on the standard deviation distribution can be observed at U_S due to the formation of a single large bubble.

Fig. 4 (c) illustrates the auto-correlation functions for three flow regimes. In the bubbling and turbulent fluidization flow regime, there is a periodic auto-correlation function on a scale and the frequency approximately equals to the corresponding dominant frequency. In the slugging flow regime, it can be seen that the decay in auto-correlation with time lag is fast. It indicates that the periodicity of the average solids volume fraction fluctuation is not significant in the slugging flow regime, which relates to the bubble dynamics.

Fig. 5 presents the power spectrum distribution calculated by Fast Flourier Transformation (FFT) for three flow regimes. It is clear that the bandwidth and amplitude vary considerably with the superficial gas velocity. Within the bubbling flow regime in Fig. 5 (a), a broad-band spectrum with low amplitude is observed, which indicates a distinguishable bubbling behavior. The dominant frequency is approximately 1 Hz. Fig. 5 (b) shows that the power spectrum for the slugging flow regime has a relatively narrow-banded spectrum with a high magnitude. This regime is governed by the dynamics of large bubbles and has much simpler signal fluctuation. The dominant frequency is relatively low (0.7 Hz). The power spectrum for the turbulent fluidization flow regime is shown in Fig. 5 (c). Compared with the slugging flow regime, the dominant frequency of turbulent fluidization flow regime is relatively high while the power spectrum magnitude is considerably low.

<Figure 4>

<Figure 5>

3.1.2 Analyses of differential pressure fluctuation

Fig. 6 shows the time domain analysis on the differential pressure fluctuations. Fig. 7 shows the power spectrum distribution for three flow regimes. Comparing Figs. 6 and 7 with Figs. 4 and 5, it can be found that the differential pressure fluctuation presents a similar behavior to the area-average solids volume fraction fluctuation. However, the transition velocities in Fig. 6 (b) (U_S' = 0.95 m/s and U_C' = 2.0 m/s) are slightly lower than those in Fig. 4 (b) (U_S = 1.1 m/s and U_C = 2.5 m/s), and the dominant frequencies are slightly higher than those of the average solids volume fraction fluctuation. One of the main reasons is that the ECT measurement represents the information on the whole cross section while the pressure probe only measures the near-wall region.

<Figure 6>

<Figure 7>

3.2 Gas-solids flow characteristics

To obtain the characteristics of the gas-solids flow, the solids volume fraction distribution and bubble characteristics obtained from the ECT sensor are further investigated.

3.2.1 Solids volume fraction distribution

The result obtained from ECT plane 1 is investigated in the riser of 10 cm in diameter with a static bed height of 25 cm. The solids volume fraction distribution is shown in Fig. 8.

The profiles of $\overline{\beta}$, $\overline{\beta}_{center}$ and $\overline{\beta}_{wall}$ with the superficial gas velocity are shown in Fig. 8 (a). The radial profile of the solids volume fraction averaged in time is shown in Fig. 8 (b). In Fig. 8 (a), $\overline{\beta}_{center}$ is the area-averaged value of $\overline{\beta}$ at the center (r/R < 0.07) and $\overline{\beta}_{wall}$ is the area-averaged value of $\overline{\beta}$ near the wall (r/R > 0.93). They are summarized from Fig. 8 (b) to investigate the maximum difference of solids volume fraction in the cross section. From Fig. 8 (a), it can be seen that $\overline{\beta}$, $\overline{\beta}_{center}$ and $\overline{\beta}_{wall}$ decrease with the superficial gas velocity. The gradients of trend lines of $\overline{\beta}$ for the three flow regimes show slightly increase. With the increase of superficial gas velocity, the difference between $\overline{\beta}_{wall}$ and $\overline{\beta}_{center}$ as a percentage of $\overline{\beta}$ increases from 9.7 % to

157 %. The above results indicate that the inhomogeneity of solids distribution in the cross section increases with the superficial gas velocity.

As shown in Fig. 8 (b), the solids volume fraction in the center is lower and increases monotonically along the radial direction towards the near wall region. In the bubbling flow regime (U < 1.1 m/s), the change in the solids volume fraction is relatively slow. The main reason is that the drag force is not strong enough to carry the highly concentrated solids in the bed when the bubble moves through the center. In the slugging flow regime (1.1 m/s < U < 2.5 m/s), the solids volume fraction in the center decreases significantly while that near the wall changes slowly. The solids volume fraction decreases by almost 40 % in the center and almost 13 % near the wall. In the turbulent fluidization flow regime, the radial profile of the solids volume fraction is similar to that of the slugging regime. The profile shows a smooth variation in the center (between r/R = 0 and r/R = 0.4) and a steep variation near the wall (between r/R = 0.4 and r/R = 1.0). This is a typical phenomenon, which can be seen in the turbulent fluidization flow regime since the gas-solids mixing increases due to the breakup of large bubbles.

<Figure 8>

3.2.2 Quasi-three-dimensional solids volume fraction distribution

Fig. 9 shows the quasi-three-dimensional distribution of solids volume fraction and the corresponding cross-sectional distribution for several typical superficial gas velocities. Each quasi-three-dimensional distribution is obtained by stacking 300 tomographic images within a consecutive period of 5 seconds. The vertical direction refers to the time. The horizontal direction refers to the diameter orientation from the top left to the bottom right of the cross-sectional images. The cross-sectional distribution in Fig. 9 represents the time-averaged solids volume fraction distributions. The color bar variation from blue to red stands for the increase of the solids volume fraction from low (empty bed) to high (close-packing).

The gas-solids flow analysis based on the quasi-three-dimensional solids volume fraction distribution is given as follows. The bubbles number in each figure stands for the frequency of bubbles through the ECT measured region, which related to bubble rising velocity. Fig. 9 (a) and (b) show the gas-solids flow behavior in the bubbling regime. A longer duration of pause between bubbles can be seen in Fig. 9 (a) and (b). In the slugging flow regime, as shown in Fig. 9 (c) and (d), there are significant differences in axial and radial distribution, compared with those in the bubbling flow regime. In addition, a growing number of bubbles can be seen and the average bubble diameter becomes larger. It should be noted that most particles tend to move to one side of the riser as a result of gas mal-distribution in plenum chamber caused by the single gas entrance at one side (Bhasker 2002). Fig. 9 (e) and (f) show the solids volume fraction distribution in the turbulent fluidization flow regime. This is the regime, in which small bubbles dominate the flow hydrodynamics. Within the cross section, the solids volume fraction in the center is much lower than that near the wall. In the meanwhile, very short duration of pause between bubbles can be observed from Fig. 9 (e) and (f).

<Figure 9>

3.2.3 Bubble diameter

Bubble size is one of the most important indexes in a fluidized bed reactor. Numerous of researches have been done in the 1970's and 1980's to investigate the bubble behavior in gas-solids fluidized beds. Darton (1977) generalized a semi-empirical model for bubble growth. The bubble diameter is defined as

$$D_b = 0.54(U - U_{mf})^{0.4}(h + 4\sqrt{\frac{A}{N_h}})^{0.8} / g^{0.2} \tag{9}$$

where D_b is the bubble diameter, h is the height of the bubble above the distributor, A is the cross-sectional area of the bed, N_h is the hole number of distributor, 0.54 is the experimentally determined constant. It was stated that this model is not applicable to slugging bed (Darton 1977).

The model defines a bubble as an area where the solids volume fraction is below a certain value. Wachem *et al*. (1998) choose this value to be 20 % of the close-packing volume fraction. When several bubbles exist in a cross section, D_b is the equivalent diameter of all bubbles in the measurement area.

Fig. 10 shows the bubble diameter obtained both by Eq. 9 and ECT for three different risers. It indicates that the bubble diameters measured by ECT plane 1 (the upper plane) are slightly larger than those obtained by Eq. 9, but they present a similar tendency with the superficial gas velocity. However, in ECT plane 2 (the lower plane), the bubble diameter measured by ECT is significantly larger than those by Darton's model. A possible reason is that the sensitivity of ECT sensor is lower in the center, which makes the ECT sensor difficult to detect small bubbles in the center.

It can be found that the measured bubble diameter in the slugging regime is different from that obtained by Eq. 9 (referencing in Fig. 10 (a): U = 1.1 m/s~2.5 m/s, Fig. 10 (b): U = 1.0 m/s~2.0 m/s and Fig. 10 (c): U = 0.8 m/s~1.9 m/s). It verifies that Darton's model is not applicable to the slugging regime.

In this research, the distributor is made of a wire mesh, which results in that the holes number in the distributor, N_h, is proportional to the cross-sectional area of the bed, A, in Eq. 9. Therefore, the bubble diameters of the three risers for the same superficial gas velocity obtained by Eq. 9 are essentially equal. This conclusion is confirmed by the ECT results that the bubble diameter has a similar value in the three different risers with the same superficial gas velocity, as shown in Fig. 10.

<Figure 10>

3.2.4 Bubble rising velocity

To investigate the bubble rising velocity, the measured results of the three different risers are analyzed using the cross-correlation method (Fan *et al*. 1983). The relationship between the signals of ECT plane 1 and plane 2 are quantified by the cross-correlation coefficient, which is used to estimate the time-lag for the bubble passing through the two planes. The gap between those two planes is 2 cm and the data acquisition rate for each plane is 60 frames per second. Compared with the bubble fluctuation frequency, i.e. less than 2.5 Hz (Fig. 4(b)), the ECT data acquisition rate is high enough to give accurate measurement results for the bubble rising velocity. It should be pointed out that the cross-correlation is only for the averaged bubbles crossing the measuring planes and it is assumed that the bubbles do not undergo too much transformation from one measuring plane to the next. The details for the calculation of the bubble rising velocity from the twin-plane ECT sensor are given by Liu *et al*. (2005).

The theoretical model proposed by Davidson and Harrison (1963) is

$$U_b = U - U_{mf} + 0.71\sqrt{gD_b} \tag{10}$$

where 0.71 is the analytically determined square root of the Froude number of a single rising bubble in an infinitely large homogeneous area in three dimensions.

The results of correlation analysis and bubble rising velocities obtained by ECT are shown in Fig. 11 (a), (c) and (e) for the three risers separately. The points with small correlation coefficients characterize that the correlation of gas-solids flow between the two adjacent planes is poor. There are two possible reasons: (1) different flow regimes exist in the two planes and (2) the gas-solids flow of the riser is unstable.

The bubble rising velocities obtained by Eq. 10 and ECT in the three risers are shown in Fig. 11 (b), (d) and (f) respectively. The bubble rising velocity obtained by Eq. 10 increases with the superficial gas velocity. The experimental results show the same distribution only in the bubbling regime for the three risers. In the bubbling regime, the bubble rising velocities obtained by Eq. 10 and ECT are approximately equal. In the slugging flow regime and turbulent fluidization flow regime, the bubble velocities become independent of the superficial gas velocity. This is consistent with the previous study by pressure fluctuation measurement (Fan *et al*. 1983). The difference between ECT measurements and the theoretical model can be explained that the visible flow rate is clearly lower than the excess gas velocity (U-U_{mf}) under normal operation conditions for bubble formation without slugging (Hilligardt and Werther 1986). Furthermore, in the turbulent fluidization flow regime there are several small bubbles in the cross section, while D_b is obtained based on the total area of bubbles instead of one bubble, thus the bubble rising velocity estimated by Eq. 10 is larger than the ECT measurement.

<Figure 11>

The hydrodynamic behavior in a gas-solids fluidized bed is a complex flow system and it is unstable due to particle acceleration, gravity and many other forces (Kariminpour and Pugsley 2011). In addition, the authors did not consider the bubble breakup and coalescence effect on the bubbling rising velocity when bubbles pass through the measuring planes (Wang and Yang 2011). The correlation calculation based on the ECT signals only give a rough estimate of the bubbling rising velocity and further work is necessary to address the above factors which affect the predicted accuracy for bubbling rising velocity.

3.3 Influence factors of transition velocities

3.3.1 Comparison of transition velocities based on H_{st}/D

Previous literature revealed that the transition velocities, U_S and U_C, are strongly depended on the ratio of the static bed height to the bed diameter (H_{st}/D) (Ellis *et al*. 2004 and Shaul *et al*. 2012). Ellis *et al*. (2004) found that U_C increases with H_{st}/D. The same result on the effect of bed diameter was also obtained by Du *et al*. (2005).

In this research, the effect of H_{st}/D on transition velocities (U_S and U_C) is investigated. A summary of experiment cases is given in Table 2. In addition, two different axial measured positions (ECT plane 1 and 2) are considered to study the effect of axial measured position. The results are shown in Fig. 12. As shown in Table 2, H_{st}/D of case 2 and case 6 are equal. The transition velocities of the two cases are almost equal in Fig. 12. It indicates that H_{st}/D as an influence factor on transition velocities is suitable for the riser in this study. In Fig. 12, the transition velocities (U_S and U_C) increase with H_{st}/D. This coincides with the previous study (Du *et al*. 2005, Ellis *et al.* 2004). As can be seen from Fig. 12, U_S is less affected by H_{st}/D than U_C. In general, the transition velocities of ECT plane 1 (upper plane) are smaller than those of ECT plane 2 (lower plane). The results indicate that with the increase of the gas velocity, the gas-solids flow at higher axial position of the riser reaches a different flow regime earlier, e.g. from bubbling regime to slugging regime. In other words, different flow regimes might exist along the riser. This was also confirmed by Rhodes *et al*. (1998) based on the analysis of gas-solids distributions both in the bottom and the top region in a fluidized bed riser.

<Table 2>

<Figure 12>

3.3.2 Comparison of transition velocities within the cross section

Bai *et al*. (1996a) reported that different local flow regimes might exist within the riser under the same superficial gas velocity. In this study, different local flow regimes in a same cross section are investigated

based on the ECT measurements. The pixels number inside the imaging area is 3001, which makes it possible to characterize the flow regimes locally. The results obtained from ECT plane 1 for the riser of 10 cm in diameter (H_{st} = 25 cm) are shown in Fig. 13. It shows the standard deviation and dominant frequency for four different radial positions. It can be seen that the standard deviation curves present a similar distribution, and the dominant frequency curves are approximately same. The transition velocities obtained from the standard deviation and dominant frequency analysis are marked with blue dotted lines in Fig. 13. It can be concluded that the transition velocities ($U_S^{"}$ and $U_C^{"}$) are nearly the same in different radial positions. The two transition velocities (0.8 m/s <$U_S^{"}$ <1.1 m/s and 2.0 m/s < $U_C^{"}$ < 2.5 m/s) are approximately equal to those (U_S = 1.1 m/s and U_C = 2.5 m/s) obtained from the average solids volume fraction in the cross section. The above results indicate that similar flow regimes might exist in different radial positions under the same operating condition.

<Figure 13>

4. Conclusions

In this research, the solids volume fractions measured by a twin-plane ECT sensor and pressure drop have been used to investigate the flow regimes in the bottom region of a CFB with different riser diameters. Time and frequency domain analysis are carried out to describe the dynamic behavior and define transition velocities. Three different flow regimes have been identified including bubbling, slugging and turbulent fluidization flow regime. The main conclusions are as follows.

(1) Gas-solids behavior in three flow regimes

In general, the average solids volume fraction within the measured cross section decreases with the superficial gas velocity. For the radial distribution, the solids volume fraction is low in the center and increases monotonically along the radial direction towards the wall region. The inhomogeneity of gas-solids flow in a cross section increases with the superficial gas velocity.

In the bubbling flow regime, bubble formation and breakup can be seen clearly. The average solids volume fraction in a cross section presents a periodic fluctuation with time. The solids volume fraction differences between different radial positions are relatively low. The standard deviation increases with the superficial gas velocity, but the dominant frequency decreases obviously.

In the slugging flow regime, the size and the number of bubble increase significantly. Thus both standard deviation and dominant frequency increase with the superficial gas velocity. The solids volume fraction decreases by almost 40 % in the center and almost 13 % near the wall. The periodicity of the average solids volume fraction in the cross section is not significant.

In the turbulent fluidization flow regime, gas-solids mixing increases due to the breakup of large bubble. The dominant frequency continues to increase while the standard deviation decreases from a maximum. The radial

profile of the solids volume fraction shows a smooth variation in the center and a steep variation near the wall.

(2) Bubble characteristics

Bubble diameter increases with the superficial gas velocity in the three flow regimes. In three risers, the bubble diameters are approximately equal under the same superficial gas velocity, because the distributor is made of a wire mesh.

The bubble rising velocity increases with the superficial gas velocity in the bubbling regime. In the slugging regime and turbulent fluidization regime, the bubble velocities become independent of the superficial gas velocity.

(3) Transition velocities (U_S and U_C)

In the bottom region of three risers, H_{st}/D as an influence factor on transition velocities is verified. Further study shows that transition velocities increase with H_{st}/D, and U_S is less affected by H_{st}/D than U_C. From the comparison studies on transition velocities in different measured positions, it can be concluded that the flow regimes at different axial heights are different. In contrast, the flow regimes within the cross section under the same operation condition might be similar to each other.

Acknowledgements

The authors are grateful to the support from the National Natural Science Foundation of China (No. 61320106004, No. 61374018) and Strategic Priority Research Program of the Chinese Academy of Sciences (No. XDA07030100).

Nomenclature

a	Area of each pixel (m^2)
A	Cross-sectional area of bed (m^2)
c_{xx}	Auto-correlation function (-)
C_H	Capacitance vector in close-packing (pf)
C_L	Capacitance vector in empty bed (pf)
C_M	Measurement capacitance vector (pf)
C_{xx}	Normalized auto-correlation function (-)
D	Inside diameter (m)
D_b	Bubble diameter (m)
g	Acceleration due to gravity (m/s^2)
G	Normalized grey level vector (-)

G^j	G obtained in *j-th* iteration (-)
h	Height of the bubble above the distributor (m)
H_{st}	Static bed height (m)
k	Δt number of time lag (-)
m_{max}	The maximum eigenvalue of S^TS(-)
M	Number of pixels in the imaging area (-)
N	ECT measurement number (-)
N_h	Number of holes in distributor (-)
r	Radial coordinate (m)
R	Riser radius (m)
S	Sensitivity matrix (-)
SD	Standard deviation (-)
Δt	Interval between ECT measurements (s)
u_λ	Identity vector (-)
U	Superficial gas velocity at the bottom of the riser (m/s)
U_C	Superficial gas velocity at the transition to turbulent fluidization regime (m/s)
U_{mf}	Critical fluidization velocity (m/s)
U_S	Superficial gas velocity at the transition to slugging regime (m/s)
Z	Axial height above the distributor (cm)

Greek symbols

α	Step length or gain factor (-)
β	Average solids volume fraction in cross section (-)
$\overline{\beta}$	Time-averaged β (-)
$\overline{\beta}_{center}$	Area-averaged $\overline{\beta}$ in the center (-)
$\overline{\beta}_{wall}$	Area-averaged $\overline{\beta}$ near the wall (-)
λ	Normalized capacitance vector (-)
θ	Close-packing volume fraction of experimental material (-)
τ	Relaxation factor (-)

References

Azzi, M., Turlier, P., Large, J.F. and Bernard, J.R. (1991), Use of a momentum probe and gamma-densitometry to study local properties of fast fluidized beds, Pergamon: Oxford, pp 189.

Bai, D., Shibuya, E., Nakagawa, N. and Kato, K. (1996a), Characterization of gas fluidization regimes using

pressure fluctuations, Powder Technology, 87, pp 105-111.

Bai, D., Shibuya, E., Masuda, Y., Nakagawa, N. and Kato, K. (1996b), Flow structure in a fast fluidized bed, Chemical Engineering Science, 51, pp 957-966.

Bhasker. C. (2002), Simulation of air flow in the typical boiler windbox segments, Advances in Engineering Software, 33, pp 793-804.

Chaplin, G., Pugsley, T., Lee, van der L., Kantzas, A. and Winters, C. (2005), The dynamic calibration of an electrical capacitance tomography sensor applied to the fluidized bed drying of pharmaceutical granule, Measurement Science and Technology, 16, pp 1281-1290.

Cui, H., Mostoufi, N. and Chaouki, J. (2001), Gas and solids between dynamic bubble and emulsion in gas-fluidized beds, Powder Technology, 120, pp 12-20.

Darton, R.C. (1977), Bubble growth due to coalescence in fluidised beds, Transactions of the Institution of Chemical Engineers, 55, pp 274-280.

Davidson, J.F. and Harrison, D. (1963), Fluidization particles, London: Cambridge University Press.

Davidson, J.F., Clift, R. and Harrison, D. (1985), Fluidization, Academic Press, London, 1985.

Depypere, F., Pieters, J.G. and Dewettinck, K. (2004), CFD analysis of air distribution in fluidised bed equipment, Powder Technology, 145, pp 176-189.

Du, B., Warsito, W. and Fan, L.S. (2005), ECT studies of gas-solid fluidized beds of different diameters, Industrial and Engineering Chemistry Research, 44, pp 5020-5030.

Dyakowski, T., Edwards, R.B., Xie, C.G. and Williams, R.A. (1997), Application of capacitance tomography to gas-solid flows, Chemical Engineering Science, 52, pp 2099-2110.

Ellis, N., Bi, H.T., Lim, C.J. and Grace, J.R. (2004), Hydrodynamics of turbulent fluidized beds of different diameters, Powder Technology, 141, pp 124-136.

Fan, L.T., Ho, T.C. and Walawender, W.P. (1983), Measurements of the rise velocities of bubbles, slugs and pressure waves in a gas-solid fluidized bed using pressure fluctuation signals, AIChE Journal, 29, pp 33-39.

Geldart, D. (1973), Types of gas fluidization, Powder Technology, 19, pp 285-292.

Hage, B., Werther, J., Narukawa, K. and Mori, S. (1996), Capacitance Probe measurement technique for local particle volume concentration in Circulating Fluidized Bed Combustors, Journal of Chemical Engineering of Japan, 29, pp 594-602.

Hilligardt, K. and Werther, J. (1986), Local bubble gas hold-up and expansion of gas/solid fluidized beds, German Chemical Engineering, 9, pp 215-221.

Johnsson, F., Zijerveld, R.C., Schouten, J.C., Van den Bleek, C.M. and Leckner, B. (2000), Characterization of fluidization regimes by time-series analysis of pressure fluctuations, International Journal of Multiphase Flow, 26, pp 663-715.

Karimipour, S. and Pugsley, T. (2011), A critical evaluation of literature correlations for predicting bubble size and velocity in gas-solid fluidized beds, Powder Technology, 205, pp 1-14.

Kim, S.W., Hirbas, G., Bi, H.T., Lim C.J. and Grace J.R. (2004), Flow behavior and regime transition in a high-density circulating fluidized bed riser, Chemical Engineering Science, 59, pp 3955-3963.

Kim, Y.S., Lee, S.H., Ijaz, U.Z., Kim, K.Y. and Choi, B.Y. (2007), Sensitivity map generation in electrical capacitance tomography using mixed normalization models, Measurement Science and Technology, 18, pp 2092-2102.

Lehner, P. and Wirth, K.E. (1999), Characterization of the flow pattern in a downer reactor, Chemical Engineering Science, 54, pp 5471-5483.

Liu, S., Chen, Q., Wang, H.G., Ismail, I. and Yang, W.Q. (2005), Electrical capacitance tomography for gas-solids flow measurement for circulating fluidized beds, Flow Measurement and Instrumentation, 16, pp 135-134.

Liu, S., Fu, L. and Yang, W.Q. (1999), Optimization of an iterative image reconstruction algorithm for electrical capacitance tomography, Measurement Science and Technology, 10, L37-L39.

Makkawi, Y.T. and Wright, P.C. (2002), Fluidization regimes in a conventional fluidized bed characterized by means of electrical capacitance tomography, Chemical Engineering Science, 57, pp 2411-2437.

Malcus, S., Chaplin, G. and Pugsley, T. (2000), The hydrodynamics of the high-density bottom zone in a CFB riser analyzed by means of electrical capacitance tomography (ECT), Chemical Engineering Science, 55, pp 4129-4138.

Monazam, E.R., Shadle, L.J. Mei, J.S. and Spenik, J. (2005), Identification and characteristics of different flow regimes in a circulating fluidized bed, Powder Technology, 155, pp 17-25.

Piskova, E. and Mörl, L. (2008), Characterization of spouted bed regimes using pressure fluctuation signals, Chemical Engineering Science, 63, pp 2307-2316.

Rhodes, M.J., Sollaart, M. and Wang, X.S. (1998), Flow structure in a fast fluid bed, Powder Technology, 99, pp 194-200.

Shaul, S., Rabinovich, E. and Kalman, H. (2012), Generalized flow regime diagram of fluidized beds based on the height to bed diameter ratio, Powder Technology, 228, pp 264-271.

Srivastava, A., Agrawal, K., Sundaresan, S., Reddy Karri, S.B. and Knowlton, T.M. (1998), Dynamics of gas-particle flow in circulating fluidized beds, Powder Technology, 100, pp 173-182.

Svensson, A., Johnsson, F. and Leckner, B. (1996), Fluidization regimes in non-slugging fluidized beds: the influence of pressure drop across the air distributor, Powder Technology, 86, pp 299-312.

van Wachem, B.G.M., Schouten, J.C., Krishna, R. and van den Bleek, C.M. (1998), Eulerian simulations of bubbling behaviour in gas-solid fluidised beds, Computers & Chemical Engineering, 22, pp S299-S306.

Wang, H.G., Senior, P.R., Mann, R. and Yang, W.Q. (2009), Online measurement and control of solids moisture in fluidised bed dryers. Chemical Engineering Science, 64, 2893-2902.

Wang, H.G., Yang, W.Q., Dyakowski, T. and Liu, S. (2006), Study of bubbling and slugging fluidized beds by simulation and ECT. AIChE Journal, 52, 3078-3087.

Wang, H.G. and Yang, W.Q. (2010), Measurement of fluidised bed dryer by different frequency and different normalisation methods with electrical capacitance tomography, Powder Technology, 199, pp 60-69.

Wang, H.G. and Yang, W.Q. (2011), Scale up of an electrical capacitance tomography sensor for imaging pharmaceutical fluidized beds and validation by computational fluid dynamics, Measurement Science and Technology, 22, no.104015.

Wang, S.J., Dyakowski, T., Xie, C.G., Williams, R.A. and Beck, M.S. (1995), Real time capacitance imaging of bubble formation at the distributor of a fluidized bed, The Chemical Engineering Journal and The Biochemical Engineering Journal, 56, pp 95-100.

Wiesendorf, V. and Werther, J. (2000), Capacitance probes for solids volume concentration and velocity measurements in industrial fluidized bed reactors, Powder Technology, 110, pp 143-157.

Yang, W.Q., Spink, D.M., York, T.A. and McCann, H. (1999), An image-reconstruction algorithm based on Landweber's iteration method for electrical-capacitance tomography, Measurement Science and Technology, 10, pp 1065-1069.

Yang, W.Q. and York, T.A., (1999), New AC-based capacitance tomography system, IEE Proc.-Sci. Meas. Technol., 146, pp 47-53.

Zijerveld, R.C., Johnsson, F., Marzocchella, A., Schouten, J.C. and van der Bleek, C.M. (1998), Fluidization regimes and transitions from fixed bed to dilute transport flow, Powder Technology, 95, pp 185-204.

Figures:

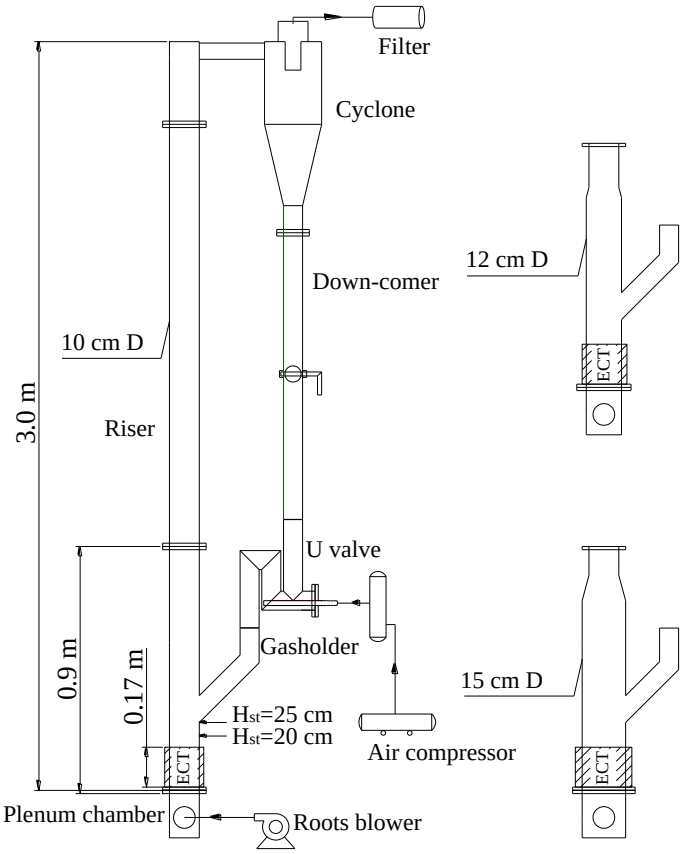

Figure 1. Circulating fluidized bed.

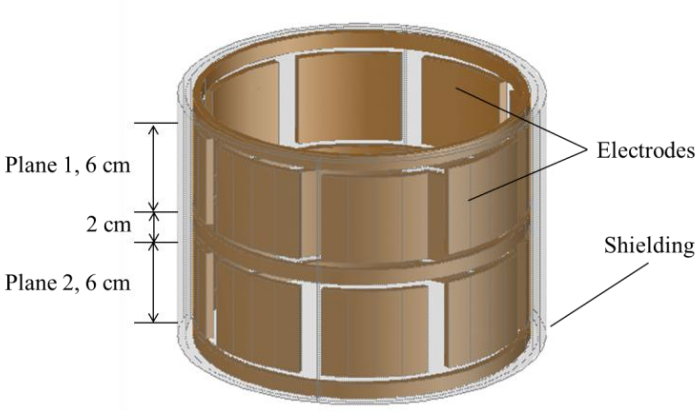

Figure 2. ECT sensor.

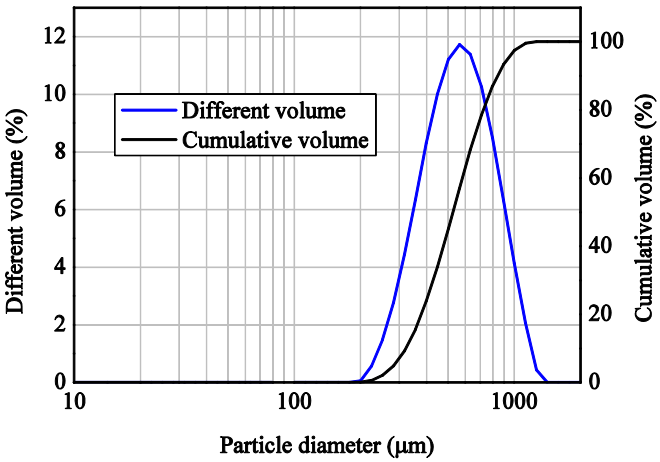

Figure 3. Particle size distribution

(a)

(b)

(c)

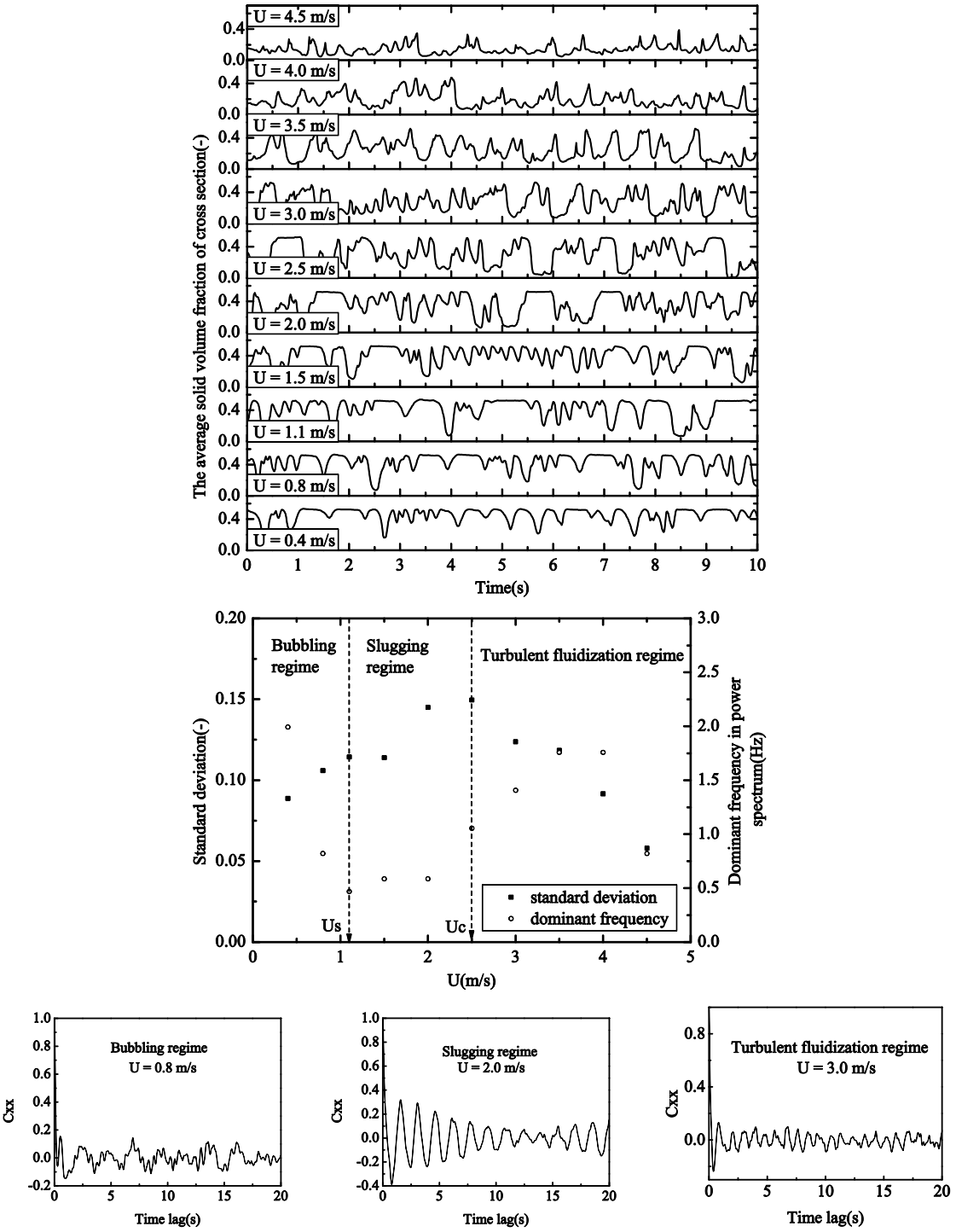

Figure 4. Time domain analysis on the solids volume fraction fluctuations for different superficial gas velocity. (a) Solids volume fraction fluctuations at different superficial gas velocity. (b) Standard deviation and dominant frequency in power spectrum of average solids volume fraction. (c) Auto-correlation coefficient.

(a)

(b)

(c)

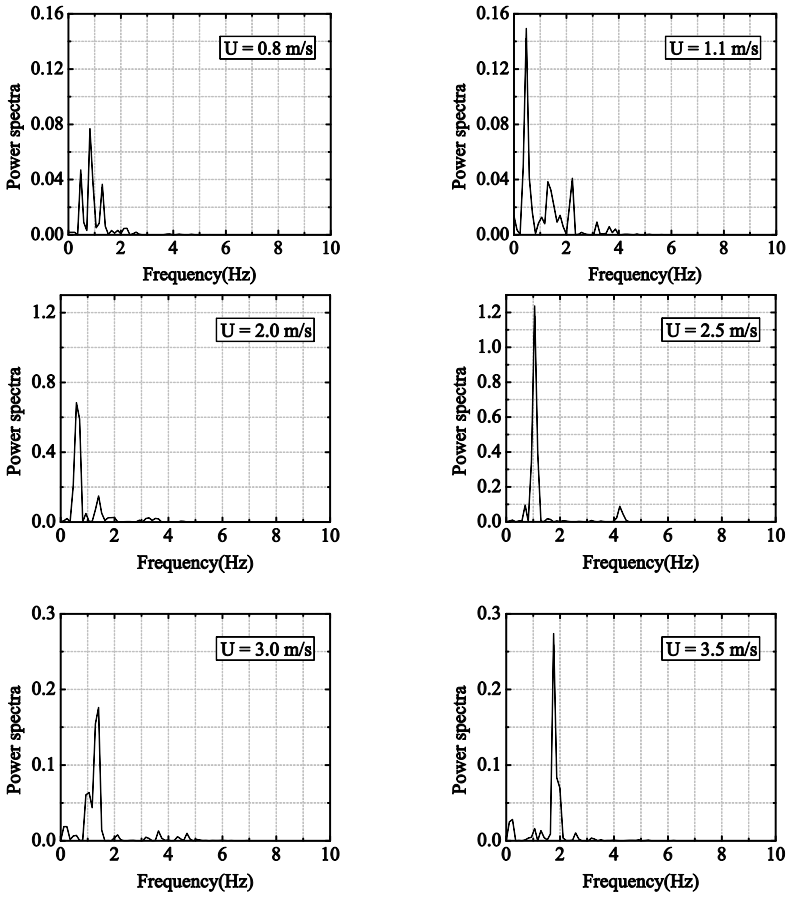

Figure 5. Power spectra of average solids volume fraction in cross section. (a) Bubbling regime. (b) Slugging regime. (c) Turbulent fluidization regime.

(a)

(b)

(c)

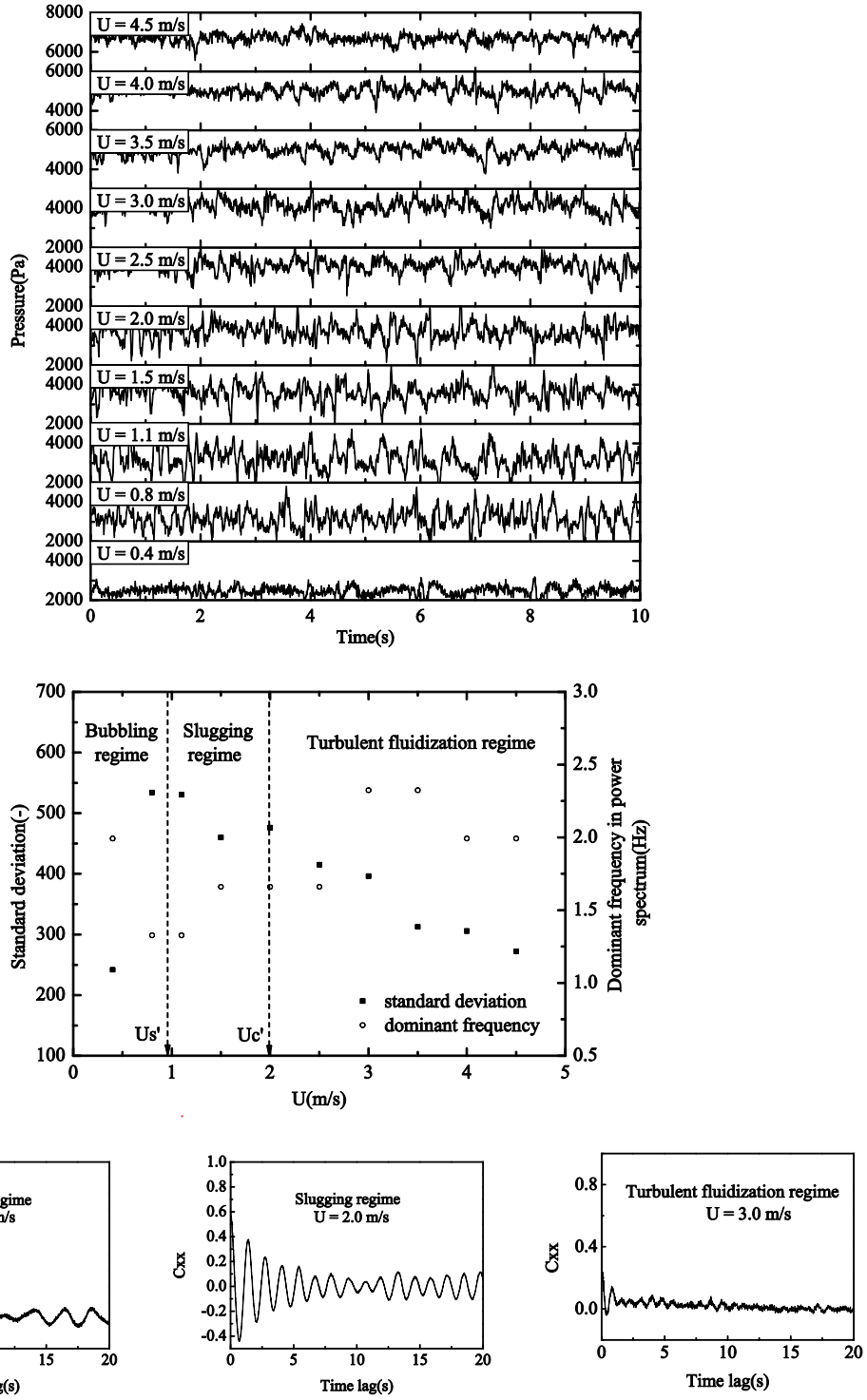

Figure 6. Time domain analysis on the differential pressure fluctuations for different superficial gas velocity. (a) Pressure fraction fluctuations at different superficial gas velocity. (b) Standard deviation and dominant frequency in power spectrum of pressure fluctuations. (c) Auto-correlation coefficient.

(a)

(b)

(c)

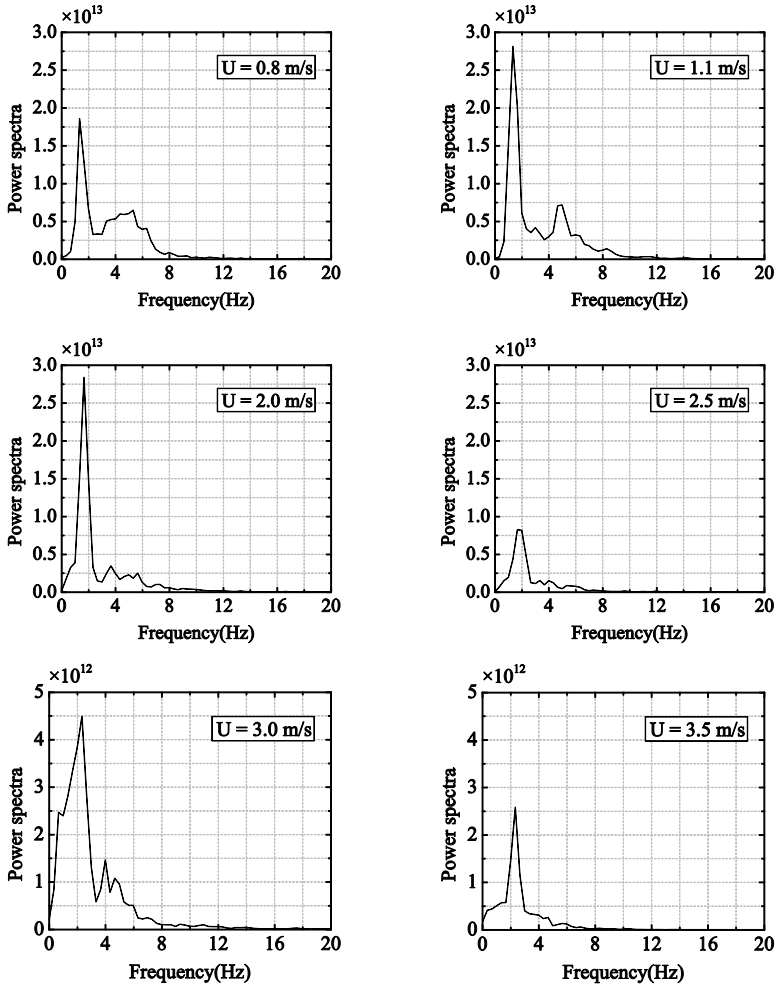

Figure 7. Power spectra of differential pressure fluctuations. (a) Bubbling regime. (b) Slugging regime. (c) Turbulent fluidization regime.

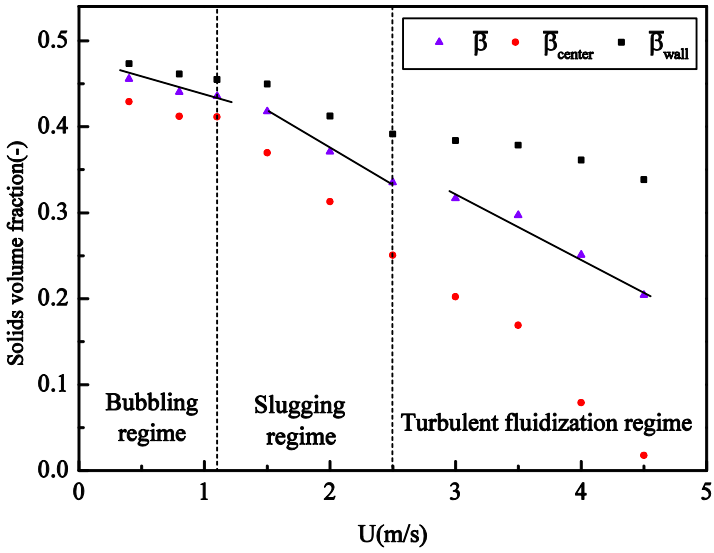

(a)

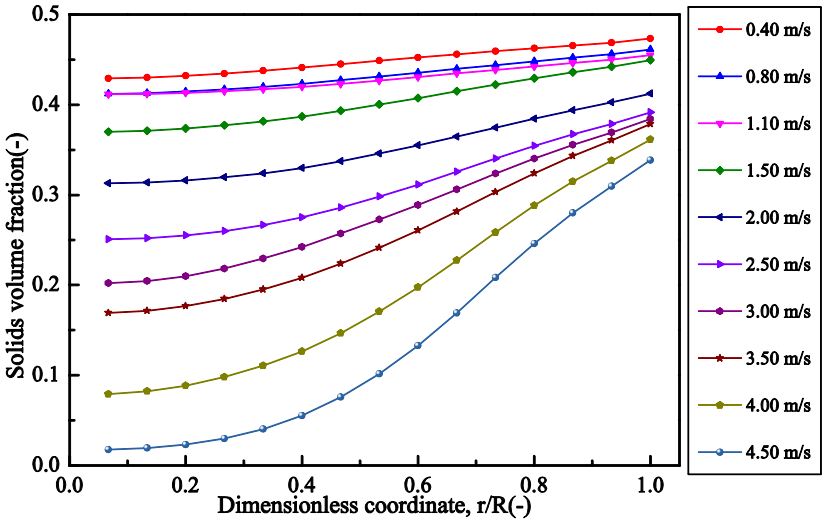

(b)

Figure 8. Solids volume fraction distribution. (a) Solids volume fraction averaged in time as a function of superficial gas velocity. (b) Radial profiles of solids volume fraction.

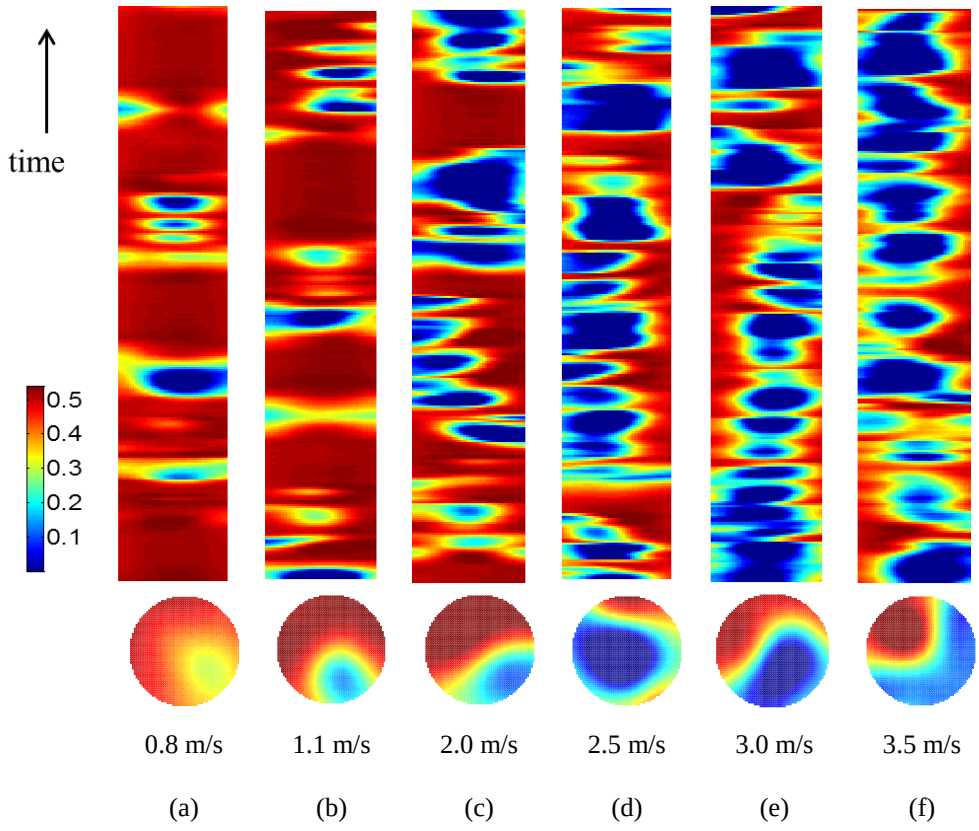

Figure 9. Quasi-three-dimensional solids volume fraction distribution.

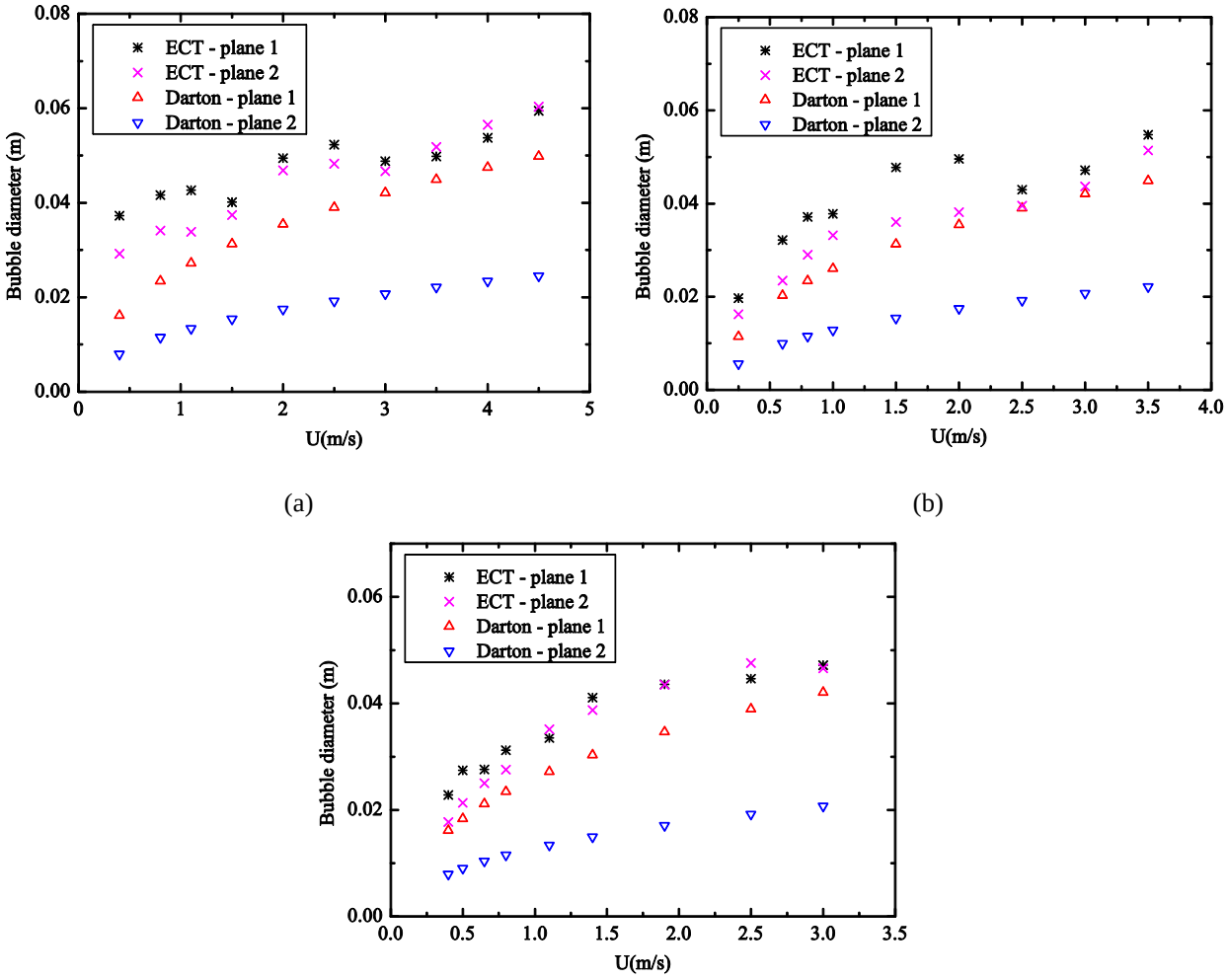

Figure 10. Bubble diameter for various gas superficial velocities. (a) 10 cm D. (b) 12 cm D. (c) 15 cm D.

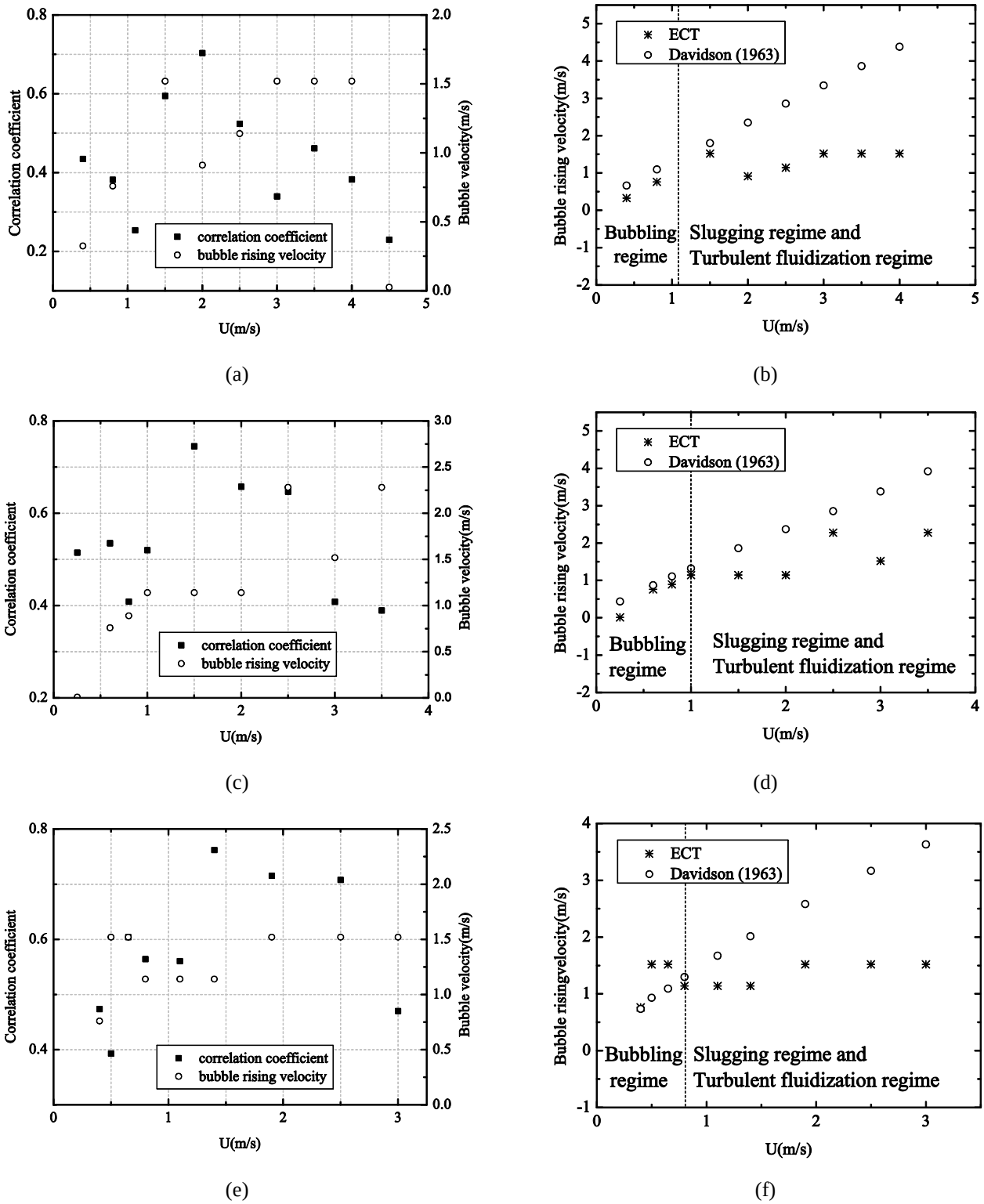

Figure 11. The results of correlation analysis and bubble rising velocity. (a) Correlation analysis for 10 cm D. (b) Bubble rising velocity for 10 cm D. (c) Correlation analysis for 12 cm D. (d) Bubble rising velocity for 12 cm D. (e) Correlation analysis for 15 cm D. (f) Bubble rising velocity for 15 cm D.

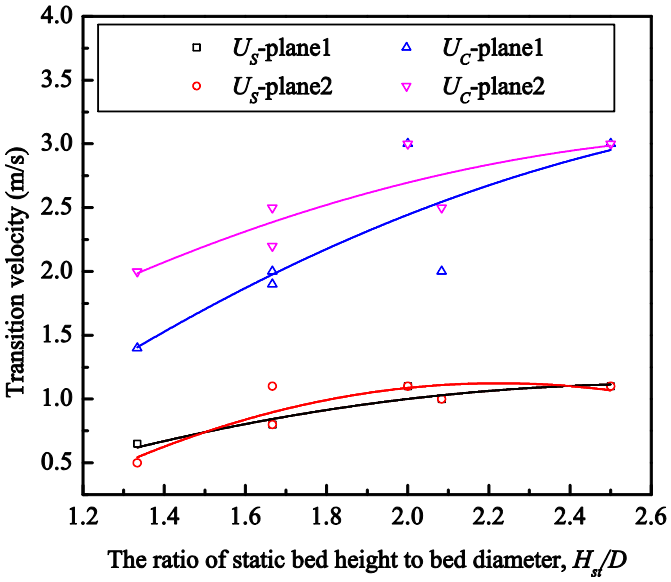

Figure 12. Transition velocity via the ratio of the static bed height to bed diameter.

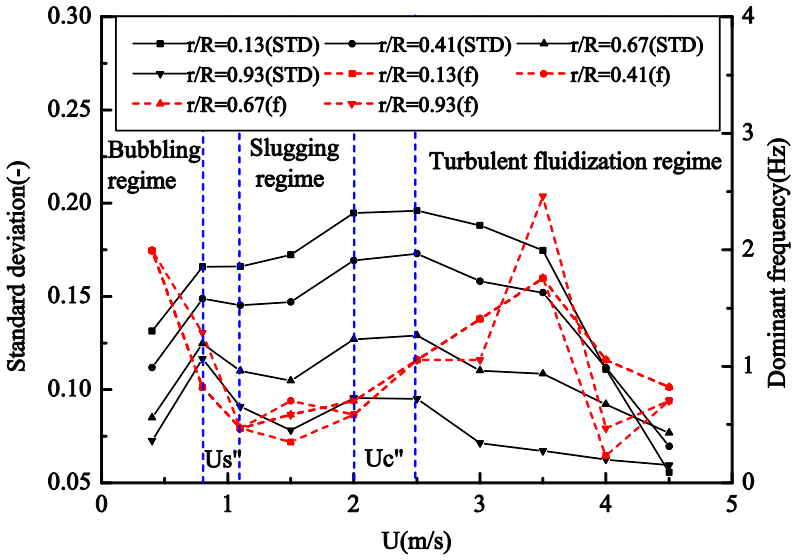

Figure 13. Radial standard deviation and dominant frequency against superficial gas velocity.

Tables:

Table 1 Summary of the experimental operation conditions

Experimental unit	Operating conditions
Riser	D = 10 cm, 12 cm, 15 cm, height = 3.0 m
Distributor	Material: wire gauze, 100 mesh, Z = 0
Fluidizing gas	Air at ambient conditions
Superficial gas velocity	0.4-4.5 m/s for 10 cm D., 0.25-3.5 m/s for 12 cm D., 0.2-3.0m/s for 15 cm D.
Particle	Material: sand, mean diameter = 469 μm, bulk density = 1608 kg/m^3
Static bed height	20 cm, 25 cm
ECT system	Plane 1: Z = 2.5-8.5 cm, plane 2: Z = 10.5-16.5 cm, eight electrodes per plane
DP transducer	Z = 2.5-16.5 cm

* Z means the axial height above the distributor

Table 2 Summary of experiment cases (H_{st}/D)

	Case 1	Case 2	Case 3	Case 4	Case 5	Case 6
H_{st}(cm)	20	20	20	25	25	25
D(cm)	10	12	15	10	12	15
H_{st}/D	2	1.67	1.33	2.5	2.08	1.67